

A Survey on 3D Gaussian Splatting

Guikun Chen, *Student Member, IEEE*, and Wenguan Wang, *Senior Member, IEEE*

Abstract—3D Gaussian splatting (3D GS) has recently emerged as a transformative technique in the explicit radiance field and computer graphics landscape. This innovative approach, characterized by the utilization of millions of 3D Gaussians, represents a significant departure from the neural radiance field (NeRF) methodologies, which predominantly use implicit, coordinate-based models to map spatial coordinates to pixel values. 3D GS, with its explicit scene representations and differentiable rendering algorithms, not only promises real-time rendering capabilities but also introduces unprecedented levels of control and editability. This positions 3D GS as a potential game-changer for the next generation of 3D reconstruction and representation. In the present paper, we provide the first systematic overview of the recent developments and critical contributions in the domain of 3D GS. We begin with a detailed exploration of the underlying principles and the driving forces behind the advent of 3D GS, setting the stage for understanding its significance. A focal point of our discussion is the practical applicability of 3D GS. By facilitating real-time performance, 3D GS opens up a plethora of applications, ranging from virtual reality to interactive media and beyond. This is complemented by a comparative analysis of leading 3D GS models, evaluated across various benchmark tasks to highlight their performance and practical utility. The survey concludes by identifying current challenges and suggesting potential avenues for future research in this domain. Through this survey, we aim to provide a valuable resource for both newcomers and seasoned researchers, fostering further exploration and advancement in applicable and explicit radiance field representation.

Index Terms—3D Gaussian Splatting, Explicit Radiance Field, Real-time Rendering, Deep Learning

1 INTRODUCTION

THE advent of neural radiance fields (NeRF) [1] marked a significant milestone in the landscape of computer graphics and 3D scene reconstruction, revolutionizing the way we approach novel-view synthesis [2]. Grounded in deep learning and computer vision, NeRF has enabled the rendering of photorealistic scenes from a sparse set of input views, establishing a new paradigm in image synthesis. However, as with any burgeoning technology, NeRF has encountered its share of challenges and limitations, particularly in terms of computational efficiency and controllability. It is in this context that 3D Gaussian splatting (3D GS) [3] emerges, not merely as an incremental improvement but as a paradigm-shifting approach that redefines the boundaries of scene representation and rendering.

The journey of novel-view synthesis began long before the introduction of NeRF, with early endeavors focusing on light fields and basic scene reconstruction methods [4]–[6]. These initial techniques, however, were limited by their reliance on dense sampling and structured capture, leading to significant challenges in handling complex scenes and lighting conditions. The emergence of structure-from-motion (SfM) [7] and subsequent advancements in multi-view stereo (MVS) [8] algorithms provided a more robust framework for 3D scene reconstruction, setting the stage for more sophisticated view synthesis algorithms. NeRF represents a quantum leap in this progression. By leveraging neural networks, NeRF enabled the mapping of spatial coordinates to color and density. The success of NeRF hinged on its ability to create continuous, volumetric scene function, producing results with unprecedented detail and

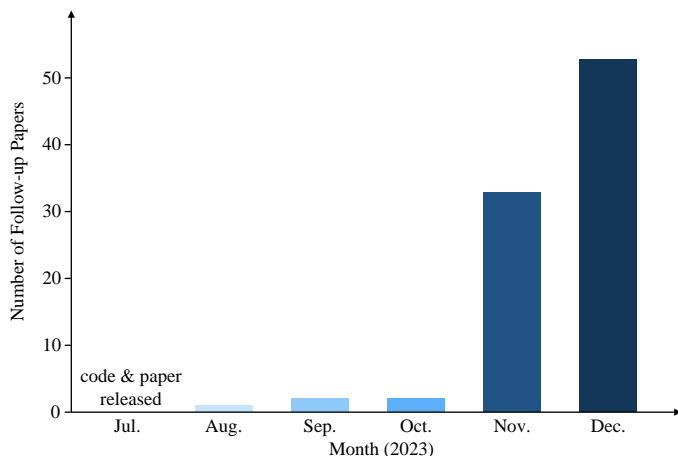


Fig. 1. The number of papers on 3D GS is increasing every month.

realism. However, this implementation came at a cost: NeRF methods were computationally intensive [9]–[14], often requiring extensive training times and substantial resources for rendering, especially for high-resolution outputs.

3D GS emerged as a response to these challenges. While NeRF excelled in creating photorealistic images, the need for faster, more efficient rendering methods was becoming increasingly apparent, especially for applications requiring real-time performance. 3D GS addressed this need by introducing a novel scene representation technique using millions of 3D Gaussians. Unlike the implicit, coordinate-based models [1], [15], [16], 3D GS employs an explicit representation and highly parallelized workflows, facilitating more efficient computation and rendering. The innovation of 3D GS lies in its unique blend of the benefits of differentiable pipelines and point-based rendering techniques [17]–[22]. By representing scenes with learnable 3D Gaussians, it

- G. Chen and W. Wang are with College of Computer Science and Technology, Zhejiang University (Email: guikun.chen@zju.edu.cn, wenguanwang.ai@gmail.com)
- Corresponding Author: Wenguan Wang

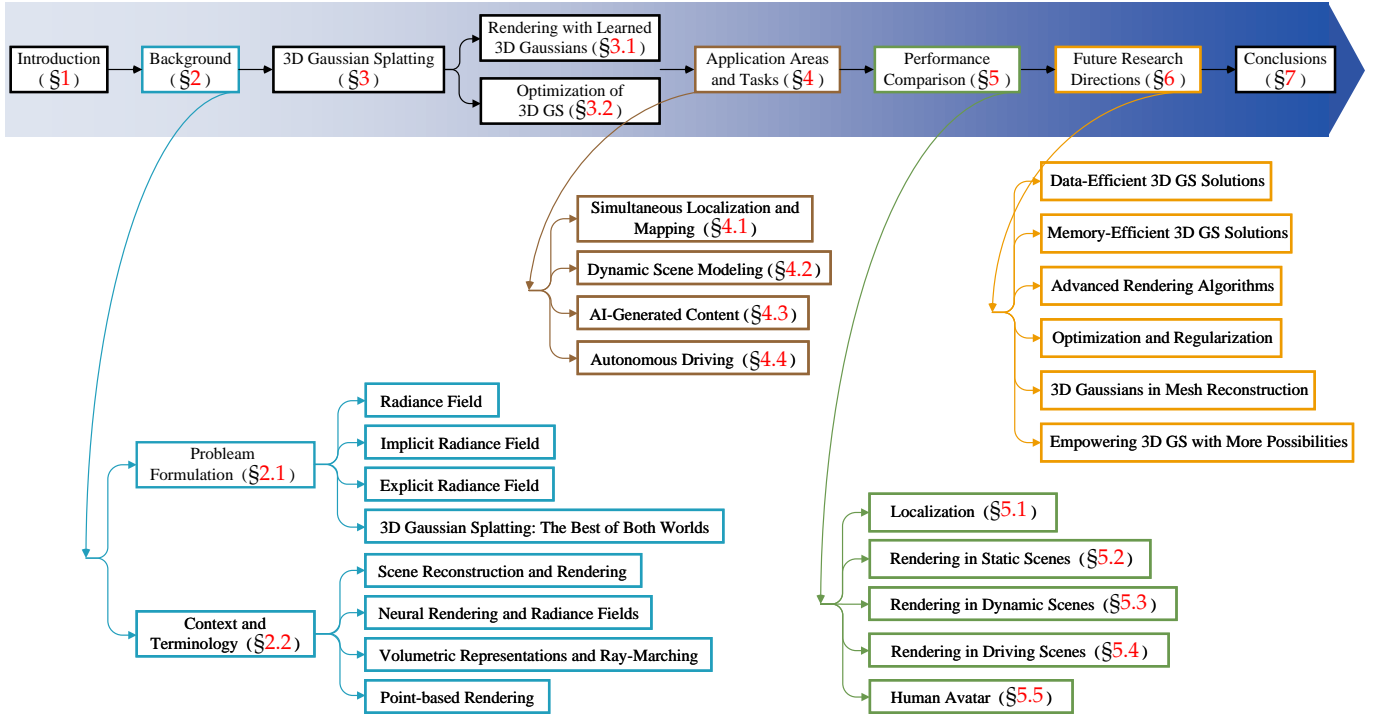


Fig. 2. Structure of the overall review.

preserves the desirable properties of continuous volumetric radiance fields, essential for high-quality image synthesis, while simultaneously avoiding the computational overhead associated with rendering in empty space, a common drawback in traditional NeRF methods.

The introduction of 3D GS is not just a technical advancement; it represents a fundamental shift in how we approach scene representation and rendering in computer graphics. By enabling real-time rendering capabilities without compromising on visual quality, 3D GS opens up a plethora of possibilities for applications ranging from virtual reality and augmented reality to real-time cinematic rendering and beyond [23], [24], [24], [25]. This technology holds the promise of not only enhancing existing applications but also enabling new ones that were previously unfeasible due to computational constraints. Furthermore, 3D GS’s explicit scene representation offers unprecedented control over scene dynamics, a crucial factor in complex scenarios involving intricate geometries and varying lighting conditions [26], [27]. This level of control and editability, combined with the efficiency of the rendering process, positions 3D GS as a transformative force in shaping future developments in the related field.

In an effort to assist readers in keeping pace with the swift evolution of 3D GS, we provide the first survey on 3D GS, which presents a systematic and timely collection of the most significant recent literature on the topic. Given that 3D GS is a very recent innovation (Fig. 1), our focus is on the diverse developments and contributions that have emerged since its introduction. The selected follow-up works of 3D GS are primarily sourced from preprints. Our primary goal is to provide a thorough and up-to-date analysis of the initial developments, theoretical foundations, and burgeoning applications of 3D GS, highlighting its potential to revolutionize the field. Acknowledging the nascent

yet rapidly evolving nature of 3D GS, this survey also aims to identify and discuss the current challenges and future prospects in the field. We offer insights into the ongoing research directions and potential advancements that 3D GS might foster. Our objective is not just to provide an academic overview but to stimulate further research and innovation in this area.

A summary of the structure of this article can be found in Fig. 2, which is presented as follows: Sec. 2 provides some brief background on problem formulation, terminology, and related research domains. Sec. 3 introduces the essential insights of 3D GS, encompassing the novel-view synthesis with 3D Gaussians and the optimization nuances of 3D GS. Sec. 4 unveils the diverse application areas and tasks where 3D GS has made significant impact, showcasing its versatility. Sec. 5 conducts performance comparisons and analysis. Finally, Sec. 6 and 7 highlights the open questions for further research and conclude the survey. We aim to provide a balanced perspective, reflecting the current scope and future potential of 3D GS, and thereby serve as a valuable resource for researchers and practitioners eager to understand and contribute to this rapidly evolving domain.

2 BACKGROUND

In this section, we first provide a brief formulation of radiance fields, a key concept in scene rendering. It outlines two main types of radiance field representations: implicit, like NeRF [1], which uses neural networks for a straightforward yet computationally demanding rendering; and explicit, like grid [28], which employs discrete structures for quicker access but at the cost of higher memory use. Sec. 2.2 further establishes linkages with relevant fields such as scene reconstruction and rendering. For a comprehensive overview about radiance fields, scene reconstruction and representa-

tion, and rendering, please see the excellent surveys [29]–[33].

2.1 Problem Formulation

2.1.1 Radiance Field

A radiance field is a representation of light distribution in a three-dimensional space, which captures how light interacts with surfaces and materials in the environment [30]. Mathematically, a radiance field can be described as a function $L : \mathbb{R}^5 \mapsto \mathbb{R}^+$, where $L(x, y, z, \theta, \phi)$ maps a point in space (x, y, z) , and a direction specified by spherical coordinates (θ, ϕ) , to a non-negative radiance value. Radiance fields can be encapsulated through implicit or explicit representations, each with specific advantages for scene representation and rendering.

2.1.2 Implicit Radiance Field

An implicit radiance field represents light distribution in a scene without explicitly defining the geometry of the scene. In the deep learning era, it often uses neural networks to learn a continuous volumetric scene representation [34], [35]. The most prominent example is NeRF [1]. In NeRF, the MLP network is used to map a set of spatial coordinates (x, y, z) and viewing directions (θ, ϕ) to color and density values. The radiance at any point is not stored explicitly but is computed on-the-fly by querying the neural network. Hence, the function can be written as:

$$L_{\text{implicit}}(x, y, z, \theta, \phi) = \text{NeuralNetwork}(x, y, z, \theta, \phi). \quad (1)$$

This format allows for a differentiable and compact representation of complex scenes, albeit often at the cost of high computational load during rendering due to volumetric ray marching [3].

2.1.3 Explicit Radiance Field

In contrast, an explicit radiance field directly represents the distribution of light in a discrete spatial structure, such as a voxel grid or a set of points [28], [36]. Each element in this structure stores the radiance information for its respective location in space. This approach allows for more direct and often faster access to radiance data but at the cost of higher memory usage and potentially lower resolution. A generic form for an explicit radiance field representation can be written as:

$$L_{\text{explicit}}(x, y, z, \theta, \phi) = \text{DataStructure}[(x, y, z)] \cdot f(\theta, \phi), \quad (2)$$

where DataStructure could be a grid or point cloud, and $f(\theta, \phi)$ is a function that modifies the radiance based on the viewing direction.

2.1.4 3D Gaussian Splatting: The Best of Both Worlds

3D GS [3] represents a shift from implicit to explicit radiance fields. It leverages the strengths of both approaches by utilizing 3D Gaussians as a flexible and efficient representation. These Gaussians are optimized to represent the scene accurately, combining the benefits of neural network-based optimization and explicit, structured data storage. This hybrid approach aims to achieve high-quality rendering with faster training and real-time performance, particularly for

complex scenes and high-resolution outputs. The 3D Gaussian representation is formulated as:

$$L_{\text{3DGS}}(x, y, z, \theta, \phi) = \sum_i G(x, y, z, \mu_i, \Sigma_i) \cdot c_i(\theta, \phi), \quad (3)$$

where G is the Gaussian function with mean μ_i and covariance Σ_i , and c represents the view-dependent color.

2.2 Context and Terminology

A number of techniques and research disciplines possess a close relationship with 3D GS, which will be described briefly in the following sections.

2.2.1 Scene Reconstruction and Rendering

Roughly speaking, scene reconstruction involves creating a 3D model of a scene from a collection of images or other data. Rendering is a more specific term which focuses on transforming computer-readable information (e.g., 3D objects in the scene) to pixel-based images. Early techniques generated realistic images based on the light fields [4]–[6]. The structure-from-motion (SfM) [7] and multi-view stereo (MVS) [8] algorithms further advanced this field by estimating 3D structures from image sequences. These historical methods set the stage for more complex scene reconstruction and rendering techniques [37]–[40].

2.2.2 Neural Rendering and Radiance Fields

Neural rendering integrates deep learning with traditional graphics techniques to create photorealistic images [41], [42]. Early attempts utilized convolutional neural networks (CNNs) for estimating blending weights [39] or texture-space solutions [43], [44]. As mentioned in Sec. 2.1.1, the radiance field represents a function which describes the amount of light traveling in every direction through every point in space. NeRFs [1], [13], [14] use neural networks to model the radiance fields, enabling detailed and realistic scene rendering.

2.2.3 Volumetric Representations and Ray-Marching

Volumetric representations model objects and scenes not just as surfaces but as volumes filled with materials or empty space [45]. This approach allows for more accurate rendering of phenomena like fog, smoke, or translucent materials. Ray-marching is a technique used with volumetric representations to render images by incrementally tracing the path of light through a volume [15], [16]. NeRF [1] shares the same spirit of volumetric ray-marching and introduce importance sampling and positional encoding to improve the quality of synthesized images. While providing high-quality results, volumetric ray-marching is computationally expensive, motivating the search for more efficient methods like 3D GS.

2.2.4 Point-based Rendering

Point-based rendering is a technique for visualizing 3D scenes using points rather than traditional polygons. This method is particularly effective for rendering complex, unstructured, or sparse geometric data. Points can be augmented with additional properties like learnable neural descriptors [46], [47], and rendered efficiently [48], [49],

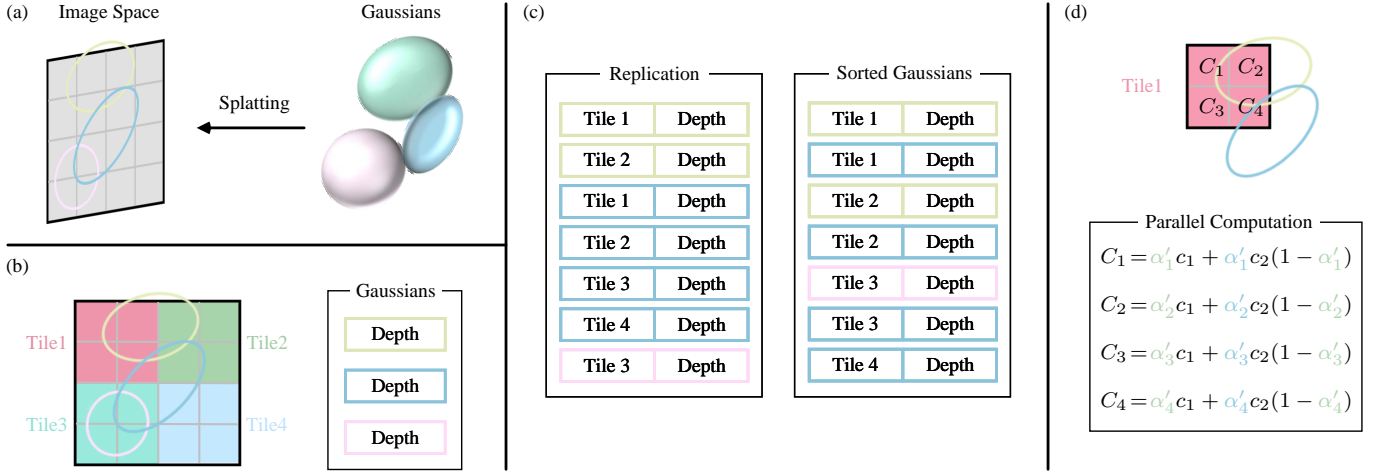


Fig. 3. An illustration of the forward process of 3D GS (Sec. 3.1). (a) The splatting step projects 3D Gaussians into image space. (b) 3D GS divides the image into multiple non-overlapping patches, *i.e.*, tiles. (c) 3D GS replicates the Gaussians which cover several tiles, assigning each copy an identifier, *i.e.*, a tile ID. (d) By rendering the sorted Gaussians, we can obtain all pixels within the tile. Note that the computational workflows for pixels and tiles are independent and can be done in parallel. Best viewed in color.

but this approach can suffer from issues like holes in the rendering or aliasing effects. 3D GS [3] extends this concept by using anisotropic Gaussians for a more continuous and cohesive representation of the scene. More details will be further discussed in Sec. 3.

3 3D GAUSSIANS FOR EXPLICIT RADIANCE FIELD

3D GS offers a breakthrough in real-time, high-resolution image rendering, without relying on neural components. This section aims to provide essential insights of 3D GS. We first elaborate how 3D GS synthesizes an image given well-constructed 3D Gaussians in Sec. 3.1, *i.e.*, the forward process of 3D GS. Then, we introduce how to obtain well-constructed 3D Gaussians for a given scene in Sec. 3.2, *i.e.*, the optimization process of 3D GS.

3.1 Novel-view Synthesis with Learned 3D Gaussians

Consider a scene represented by (millions of) optimized 3D Gaussians. The objective is to generate an image from a specified camera pose. Recall that NeRFs approach this task through computationally demanding volumetric ray-marching, sampling 3D space points per pixel. Such a paradigm struggles with high-resolution image synthesis, failing to achieve real-time rendering speeds [3]. By sharp contrast, 3D GS begins by projecting these 3D Gaussians onto a pixel-based image plane, a process termed “splatting” (Fig. 3a). Afterwards, 3D GS sorts these Gaussians and computes the value for each pixel. As seen, the rendering of NeRFs and 3D GS can be viewed as an inverse process of each other. In what follows, we begin with the definition of a 3D Gaussian, which is the minimal element of the scene representation in 3D GS. Next, we describe how these 3D Gaussians can be used for differentiable rendering. Finally, we introduce the acceleration techniques used in 3D GS, which is the key to fast rendering.

• **Properties of 3D Gaussian.** A 3D Gaussian is characterized by its center (position) μ , opacity α , 3D covariance matrix Σ , and color c . c is represented by spherical harmonics for view-dependent appearance. All the properties are learnable and optimized through back-propagation.

• **Frustum Culling.** Given a specified camera pose, this step determines which 3D Gaussians are outside the camera’s frustum. By doing so, 3D Gaussians outside the given view will not be involved in the subsequent computation, thus saving computational resources.

• **Splatting.** In this step, 3D Gaussians (ellipsoids) are projected into the 2D image space (ellipses) for rendering. Given the viewing transformation W and 3D covariance matrix Σ , the projected 2D covariance matrix Σ' is computed using:

$$\Sigma' = JW\Sigma W^\top J^\top, \quad (4)$$

where J is the Jacobian of the affine approximation of the projective transformation [3], [50].

• **Rendering by Pixels.** Before delving into the final version of 3D GS which utilizes several techniques to boost parallel computation, we first elaborate its simpler form to offer insights into its working mechanism. Given the position of a pixel x , its distance to all overlapping Gaussians, *i.e.*, the depths of these Gaussians, can be computed through the viewing transformation W , forming a sorted list of Gaussians \mathcal{N} . Then, alpha compositing is adopted to compute the final color of this pixel:

$$C = \sum_{i \in \mathcal{N}} c_i \alpha'_i \prod_{j=1}^{i-1} (1 - \alpha'_j), \quad (5)$$

where c_i is the learned color and the final opacity α'_i is the multiplication result of the learned opacity α_i and the Gaussian:

$$\alpha'_i = \alpha_i \times \exp\left(-\frac{1}{2}(x' - \mu'_i)^\top \Sigma_i'^{-1}(x' - \mu'_i)\right), \quad (6)$$

where x' and μ'_i are coordinates in the projected space. It is a reasonable concern that the rendering process described could be slower compared to NeRFs, given that generating the required sorted list is hard to parallelize. Indeed, this concern is justified; rendering speeds can be significantly impacted when utilizing such a simplistic, pixel-by-pixel approach. To achieve real-time rendering, 3D GS makes several concessions to accommodate parallel computation.

- **Tiles (Patches).** To avoid the cost computation of deriving Gaussians for each pixel, 3D GS shifts the precision from pixel-level to patch-level detail. Concretely, 3D GS initially divides the image into multiple non-overlapping patches, called “tiles” in the original paper [3]. Fig. 3b provides an illustration of tiles. Each tile comprises 16×16 pixels as suggested in [3]. 3D GS further determines which tiles intersect with these projected Gaussians. Given that a projected Gaussian may cover several tiles, a logical method involves replicating the Gaussian, assigning each copy an identifier (*i.e.*, a tile ID) for the relevant tile.

- **Parallel Rendering.** After replication, 3D GS combines the respective tile ID with the depth value obtained from the view transformation for each Gaussian. This results in an unsorted list of bytes where the upper bits represent the tile ID and the lower bits signify depth. By doing so, the sorted list can be directly utilized for rendering (*i.e.*, alpha compositing). Fig. 3c and Fig. 3d provide the visual demonstration of such concepts. It’s worth highlighting that rendering each tile and pixel occurs **independently**, making this process highly suitable for parallel computations. An additional benefit is that each tile’s pixels can access a common **shared memory** and maintain a **uniform read sequence**, enabling parallel execution of alpha compositing with increased efficiency. In the official implementation of the original paper [3], the framework regards the processing of tiles and pixels as analogous to the blocks and threads, respectively, in CUDA programming architecture.

In a nutshell, 3D GS introduces several approximations during the forward processing phase to enhance computational efficiency while maintaining a high standard of image synthesis quality.

3.2 Optimization of 3D Gaussian Splatting

At the heart of 3D GS lies an optimization procedure devised to construct a copious collection of 3D Gaussians that accurately captures the scene’s essence, thereby facilitating free-viewpoint rendering. On the one hand, the properties of 3D Gaussians should be optimized via differentiable rendering to fit the textures of a given scene. On the other hand, the number of 3D Gaussians that can represent a given scene well is unknown in advance. One promising avenue is to let the neural network automatically learn the density of 3D Gaussians. We will introduce how to optimize the properties of each Gaussian in Sec. 3.2.1 and how to control the density of the Gaussians in Sec. 3.2.2. The two procedures are interleaved within the optimization workflow. Since there are many manually set hyperparameters in the optimization process, we omit the notations of most hyperparameters for clarity.

3.2.1 Parameter Optimization

- **Loss Function.** Once the synthesis of the image is complete, the loss is calculated as the difference between the rendered image and ground truth:

$$\mathcal{L} = (1 - \lambda)\mathcal{L}_1 + \lambda\mathcal{L}_{D-SSIM}, \quad (7)$$

where λ is a weighting factor. \mathcal{L}_1 loss and D-SSIM term are standard measures. The loss function of 3D GS is slightly different from that of NeRFs. NeRFs typically calculate at

the pixel level rather than the image level because of the costly ray-marching.

- **Parameter Update.** Most properties of a 3D Gaussian can be optimized directly through back-propagation. It is essential to note that directly optimizing the covariance matrix Σ can result in a non-positive semi-definite matrix, which would not adhere to the physical interpretation typically associated with covariance matrices. To circumvent this issue, 3D GS chooses to optimize a quaternion q and a 3D vector s . q and s represent rotation and scale, respectively. This approach allows the covariance matrix Σ to be reconstructed as follows:

$$\Sigma = RSS^\top R^\top, \quad (8)$$

where R and S denote the rotation and scaling matrix derived from q and s , respectively. There is a complex computational graph to obtain the opacity α , *i.e.*, q and $s \mapsto \Sigma$, $\Sigma \mapsto \Sigma'$, and $\Sigma' \mapsto \alpha$. To avoid the cost of automatic differentiation, 3D GS derives the gradients for q and s so as to compute them directly during optimization.

3.2.2 Density Control

- **Initialization.** 3D GS starts with the initial set of sparse points from SfM or random initialization. Afterwards, point densification and pruning are adopted to control the density of 3D Gaussians.

- **Point Densification.** In the point densification phase, 3D GS adaptively increases the density of Gaussians to better capture the details of a scene. This process is particularly focused on areas with missing geometric features or regions where Gaussians are too spread out. The densification performs after a certain number of iterations, targeting Gaussians exhibiting large view-space positional gradients (*i.e.*, above a specific threshold). It involves either cloning small Gaussians in under-reconstructed areas or splitting large Gaussians in over-reconstructed regions. For cloning, a copy of the Gaussian is created and moved towards the positional gradient. For splitting, a large Gaussian is replaced with two smaller ones, reducing their scale by a specific factor. This step seeks to an optimal distribution and representation of Gaussians in the 3D space, enhancing the overall quality of the reconstruction.

- **Point Pruning.** The point pruning stage involves the removal of superfluous or less impactful Gaussians, which can be viewed as a regularization process to some extent. This step is executed by eliminating Gaussians that are virtually transparent (with α below a specified threshold) and those that are excessively large in either world-space or view-space. In addition, to prevent unjustified increases in Gaussian density near input cameras, the alpha value of the Gaussians is set close to zero after a certain number of iterations. This allows for a controlled increase in the density of necessary Gaussians while enabling the culling of redundant ones. The process not only helps in conserving computational resources but also ensures that the Gaussians in the model remain precise and effective for the representation of the scene.

4 APPLICATION AREAS AND TASKS

The transformative potential of 3D GS extends far beyond its theoretical and computational advancements. This section

dives into the diverse and groundbreaking application areas where 3D GS is making a significant impact, such as robotics, scene reconstruction and representation, AI-generated content, autonomous driving, and even other scientific disciplines. The applications of 3D GS demonstrate its versatility and potential to revolutionize various fields. Here, we outline some of the most notable application domains, providing insights into how 3D GS is shaping new frontiers in each area.

4.1 Simultaneous Localization and Mapping (SLAM)

SLAM is a computational problem central to robotics and autonomous systems. It involves the challenge of a robot or a device understanding its position in an unknown environment while simultaneously mapping the environment's layout [51]. SLAM is critical in various applications, including autonomous vehicles, augmented reality, and robotic navigation [52], [53]. The core of SLAM is to create a map of an unknown environment and determine the device's location on this map in real-time. As a result, SLAM poses great challenges for computationally intensive scene representation techniques, yet serves as a good testbed for 3D GS.

3D GS enters the SLAM domain as an innovative approach for scene representation. Traditional SLAM systems often use point/surfel clouds or voxel grids to represent environments [54]–[61]. In contrast, 3D GS utilizes anisotropic Gaussians to better represent environments. This representation offers several benefits: 1) Efficiency: The density of 3D Gaussians is adaptively controlled so as to compactly represent spatial data, reducing computational load. 2) Accuracy: The anisotropic Gaussians allows for more detailed and accurate environment modeling, especially beneficial in complex or dynamically changing scenes. 3) Adaptability: 3D GS can be adapted for various scales and complexities of environments, making it versatile for different SLAM applications. Several innovative studies have employed 3D Gaussian Splatting in SLAM [62]–[66], showcasing the potential and versatility of this paradigm. For instance, GS-SLAM [65] introduces 3D Gaussians for scene representation in the SLAM system. The method focuses on balancing efficiency and accuracy, significantly improving map optimization and re-rendering processes in RGB-D mapping. SplatAM [66] demonstrates using 3D Gaussians for dense SLAM with a single unposed monocular RGB-D camera. It addresses limitations of prior representations, offering improvements in rendering speed and map accuracy. Integrating neural rendering with SLAM, Photo-SLAM [62] utilizes 3D GS for efficient and high-quality mapping. It showcases significant improvements in photorealistic mapping and rendering speeds, particularly on portable devices. 3D GS also demonstrates impressive results in modeling dynamic urban scenes [67], [68].

4.2 Dynamic Scene Modeling

Dynamic scene modeling refers to the process of capturing and representing the three-dimensional structure and appearance of a scene that changes over time [69]–[72]. This involves creating a digital model that accurately reflects the geometry, motion, and visual aspects of the objects in the

scene as they evolve. Dynamic scene modeling is crucial in various applications, including virtual and augmented reality, 3D animation, and computer vision. 4D Gaussian Splatting (4D GS) [73]–[75] extends the concept of 3D GS to dynamic scenes. It incorporates the temporal dimension, allowing for the representation and rendering of scenes that change over time. This paradigm offers significant improvements in rendering dynamic scenes in real-time while maintaining high-quality visual outputs. For instance, [73], [74] focus on extending 3D GS to model dynamic scenes. They introduce methods for tracking and representing moving scene elements. [76]–[81] present deformable or motion models to do so. [82]–[84] explore novel applications and editing capabilities in dynamic scenes. They introduce innovative frameworks for manipulating and editing dynamic content in 4D space, demonstrating the versatility of Gaussian splatting in creative and interactive scenarios. [76], [85] emphasize improving efficiency and real-time performance. They propose optimized methods for faster rendering and reduced memory usage, making Gaussian splatting more practical for real-world applications. [86] introduces advanced rendering techniques that enhance the quality and speed of dynamic scene modeling. It focuses on optimizing the representation and rendering pipeline to achieve high-resolution, photorealistic results in real-time.

4.3 AI-Generated Content (AIGC)

AIGC refers to the digital content that is autonomously created or significantly altered by artificial intelligence systems, particularly in the fields of computer vision, natural language processing, and machine learning. AIGC is characterized by its ability to simulate, extend, or augment human-generated content, enabling applications that range from realistic image synthesis to dynamic narrative creation. The significance of AIGC lies in its transformative potential across various sectors, including entertainment, education, and technology development [87]–[90]. It's a pivotal element in the evolving landscape of digital content creation, offering scalable, customizable, and often more efficient alternatives to traditional methods.

This explicit nature of 3D GS facilitates real-time rendering capabilities and unprecedented levels of control and editability, making it highly relevant for AIGC applications. The explicit scene representations and differentiable rendering algorithms of 3D GS align perfectly with the requirements of AIGC for generating high-fidelity, real-time, and editable content, crucial for applications in virtual reality, interactive media, and beyond. Several recent works have effectively utilized 3D GS in conjunction with fields like generative models [91]–[105], avatars [106]–[128], and scene editing [82]–[84], [129]–[135]. For instance, [91] generates high-quality 3D objects using Gaussian splatting based text-to-3D generation. [125] focuses on creating animatable human avatars from monocular videos, a significant advancement in AIGC and achieves real-time rendering frame rates (50+ FPS). [132] extends the capabilities of 3D GS to include segmentation and editing in open-world 3D scenes. [131] exemplifies the use of 3D GS for interactive scene manipulation and inpainting while [130] demonstrates similar editability with text instructions.

TABLE 1

Quantitative localization results (§5.1) on Replica [136], in terms of absolute trajectory error (ATE, cm). * denotes numbers taken from [64]. (The three best scores are marked in **red**, **blue**, and **green**, respectively. These notes also apply to the other tables.)

Method	3D GS	Room0	Room1	Room2	Office0	Office1	Office2	Office3	Office4	Average
F2F* [137] [ICCV17]		1.64	1.92	2.80	2.48	0.80	4.55	2.64	2.27	2.38
iMAP [138] [ICCV21]		3.12	2.54	2.31	1.69	1.03	3.99	4.05	1.93	2.58
Vox-Fusion [139] [ISMAR22]		1.37	4.70	1.47	8.48	2.04	2.58	1.11	2.94	3.09
NICE-SLAM [140] [CVPR22]		0.97	1.31	1.07	0.88	1.00	1.06	1.10	1.13	1.06
ESLAM [141] [CVPR23]		0.71	0.70	0.52	0.57	0.55	0.58	0.72	0.63	0.63
Point-SLAM [142] [ICCV23]		0.61	0.41	0.37	0.38	0.48	0.54	0.69	0.72	0.52
Co-SLAM [143] [CVPR23]		0.70	0.95	1.35	0.59	0.55	2.03	1.56	0.72	1.00
F2GM+F2F [64] [arXiv]	✓	3.35	8.74	3.13	1.11	0.81	0.78	1.08	7.21	3.27
GSSLAM [63] [arXiv]	✓	0.47	0.43	0.31	0.70	0.57	0.31	0.31	3.20	0.79
SplaTAM [66] [arXiv]	✓	0.31	0.40	0.29	0.47	0.27	0.29	0.32	0.55	0.36
GS-SLAM [65] [arXiv]	✓	0.48	0.53	0.33	0.52	0.41	0.59	0.46	0.70	0.50

4.4 Autonomous Driving

Autonomous driving aims to allow vehicles to navigate and operate without human intervention. These vehicles are equipped with a suite of sensors, including cameras, light detection and ranging (LiDAR), and radar, combined with advanced algorithms, machine learning models, and significant computational power [144]–[147]. The central aim is to perceive the environment, make informed decisions, and execute maneuvers safely and efficiently [148]–[151]. Autonomous driving holds transformative potential for transportation, offering key benefits such as improved road safety by reducing human error, enhanced mobility for those unable to drive, and optimized traffic flow leading to reduced congestion and environmental impact [152].

Autonomous vehicles need to perceive and interpret their surroundings to navigate safely. This involves reconstructing the driving scene in real-time, accurately identifying static and dynamic objects, and understanding their spatial relationships and movements [153]–[155]. In dynamic driving scenes, the environment is continuously changing due to moving objects like other vehicles, pedestrians, or animals [156]. Accurately reconstructing these scenes in real-time is crucial for safe navigation but is challenging due to the complexity and variability of the elements involved. In autonomous driving, 3D GS can be utilized to reconstruct a scene by blending data points (such as those obtained from sensors like LiDAR) into a cohesive and continuous representation. This is particularly useful for handling the varying densities of data points and ensuring a smooth and accurate reconstruction of both the static background and dynamic objects in a scene. To date, few works [68], [157] has modeled dynamic driving/street scenes with 3D Gaussians and demonstrates superior performance in scene reconstruction compared to existing methods.

5 PERFORMANCE COMPARISON

In this section, we provide more empirical evidence by presenting the performance of several 3D GS algorithms that we previously discussed. The diverse applications of 3D GS across numerous tasks, coupled with the custom-tailored algorithmic designs for each task, render a uniform comparison of all 3D GS algorithms across a single task or dataset impracticable. Therefore, drawing from our analysis in Sec. 4, we have chosen three representative tasks within the 3D GS domain for an in-depth performance evaluation. The performance scores are primarily sourced from the original papers, except where indicated otherwise.

5.1 Performance Benchmarking: Localization

The localization task in SLAM involves determining the precise position and orientation of a robot or device within an environment, typically using sensor data.

- **Dataset:** The Replica [136] dataset is a collection of 18 highly detailed 3D indoor scenes, designed for advancing research in various machine learning and computer vision areas. These scenes are not only visually realistic but also offer comprehensive data including dense meshes, high-quality HDR textures, and detailed semantic information for each element. Following [138], three sequences about rooms and five sequences about offices are used for the evaluation.

- **Benchmarking Algorithms:** For performance comparison, we involve four recent papers which introduce 3D Gaussians into their systems (*i.e.*, Gaussian-SLAM [64], GSSLAM [63], SplaTAM [66], and GS-SLAM [65]), as well as seven typical SLAM methods (*i.e.*, F2F [137], iMAP [138], Vox-Fusion [139], NICE-SLAM [140], ESLAM [141], Point-SLAM [142], and Co-SLAM [143]).

- **Evaluation Metric:** The root mean square error (RMSE) of the absolute trajectory error (ATE) is a commonly used metric in evaluating SLAM systems [158], measuring the root mean square of the Euclidean distances between the estimated and true positions over the entire trajectory of the robot or device.

- **Result:** As shown in Table 1, the recent 3D Gaussians based localization algorithms has a clear advantage over existing NeRF based dense visual SLAM. For example, SplaTAM [66] achieves a trajectory error improvement of over 30%, decreasing it from 0.52cm to **0.36cm** compared to the previous state-of-the-art (SOTA) [142]. This confirms the efficacy of representing scenes with 3D Gaussians in the localization task.

5.2 Performance Benchmarking: Rendering in Static Scenes

Rendering focuses on transforming computer-readable information (*e.g.*, 3D objects in the scene) to pixel-based images. Here we aim to evaluate the quality of rendering results for a given pose.

- **Dataset:** The same dataset as in Sec. 5.1, *i.e.*, Replica [136], is used for performance comparison.

- **Benchmarking Algorithms:** For performance comparison, we involve four recent papers which introduce 3D Gaussians into their systems (*i.e.*, Gaussian-SLAM [64], GSSLAM [63], SplaTAM [66], and GS-SLAM [65]), as well as

TABLE 2

Quantitative rendering results (§5.2) on Replica [136], in terms of PSNR, SSIM, and LPIPS. The numbers of FPS are taken from [63].

Method	3D GS	Metric	Room0	Room1	Room2	Office0	Office1	Office2	Office3	Office4	Average	FPS
NICE-SLAM [140] [CVPR22]		PSNR↑	22.12	22.47	24.52	29.07	30.34	19.66	22.23	24.94	24.42	0.54
		SSIM↑	0.69	0.76	0.81	0.87	0.89	0.80	0.80	0.86	0.81	
		LPIPS↓	0.33	0.27	0.21	0.23	0.18	0.23	0.21	0.20	0.23	
Vox-Fusion [139] [ISMAR22]		PSNR↑	22.39	22.36	23.92	27.79	29.83	20.33	23.47	25.21	24.41	2.17
		SSIM↑	0.68	0.75	0.80	0.86	0.88	0.79	0.80	0.85	0.80	
		LPIPS↓	0.30	0.27	0.23	0.24	0.18	0.24	0.21	0.20	0.24	
Point-SLAM [142] [ICCV23]		PSNR↑	32.40	34.08	35.50	38.26	39.16	33.99	33.48	33.49	35.17	1.33
		SSIM↑	0.97	0.98	0.98	0.98	0.99	0.96	0.96	0.98	0.97	
		LPIPS↓	0.11	0.12	0.11	0.10	0.12	0.16	0.13	0.14	0.12	
Gaussian-SLAM [64] [arXiv]	✓	PSNR↑	34.31	37.28	38.18	43.97	43.56	37.39	36.48	40.19	38.90	-
		SSIM↑	0.99	0.99	0.99	1.00	0.99	0.99	0.99	1.00	0.99	
		LPIPS↓	0.08	0.07	0.07	0.04	0.07	0.08	0.08	0.07	0.07	
GSSLAM [63] [arXiv]	✓	PSNR↑	34.83	36.43	37.49	39.95	42.09	36.24	36.70	36.07	37.50	769
		SSIM↑	0.95	0.96	0.96	0.97	0.98	0.96	0.96	0.96	0.96	
		LPIPS↓	0.07	0.08	0.07	0.07	0.06	0.08	0.07	0.10	0.07	
SplaTAM [66] [arXiv]	✓	PSNR↑	32.86	33.89	35.25	38.26	39.17	31.97	29.70	31.81	34.11	-
		SSIM↑	0.98	0.97	0.98	0.98	0.98	0.97	0.95	0.95	0.97	
		LPIPS↓	0.07	0.10	0.08	0.09	0.09	0.10	0.12	0.15	0.10	
GS-SLAM [65] [arXiv]	✓	PSNR↑	31.56	32.86	32.59	38.70	41.17	32.36	32.03	32.92	34.27	-
		SSIM↑	0.97	0.97	0.97	0.99	0.99	0.98	0.97	0.97	0.97	
		LPIPS↓	0.09	0.07	0.09	0.05	0.03	0.09	0.11	0.11	0.08	

TABLE 3

Quantitative rendering results (§5.3) on D-NeRF [69], in terms of PSNR, SSIM, and LPIPS. * denotes numbers taken from [73].

Method	3D GS	PSNR↑	SSIM↑	LPIPS↓
D-NeRF [69] [CVPR21]		30.50	0.95	0.07
TiNeuVox-B [159] [SGA22]		32.67	0.97	0.04
KPlanes [36] [CVPR23]		31.61	0.97	-
HexPlane-Slim [160] [CVPR23]		32.68	0.97	0.02
FFDNeRF [72] [ICCV23]		32.68	0.97	0.02
MSTH [161] [NeurIPS23]		31.34	0.98	0.02
3D GS* [3] [TOG23]	✓	23.19	0.93	0.08
CoGS [84] [arXiv]	✓	37.90	0.98	0.02
4D-GS [73] [arXiv]	✓	34.05	0.98	0.02
GauFRé [76] [arXiv]	✓	34.80	0.98	0.02
4DGS [75] [arXiv]	✓	34.09	0.98	-

three dense SLAM methods (*i.e.*, NICE-SLAM [140], Vox-Fusion [139], and Point-SLAM [142]).

- **Evaluation Metric:** Peak signal-to-noise ratio (PSNR), structural similarity (SSIM) [162], and learned perceptual image patch similarity (LPIPS) [163] are used for measuring RGB rendering performance.

- **Result:** Table 2 shows that 3D Gaussians based systems generally outperform the three dense SLAM competitors. For example, Gaussian-SLAM [64] establishes new SOTA and outperforms previous methods by a large margin. Compared to Point-SLAM [142], GSSLAM [63] is about 578 times faster in achieving very competitive accuracy. This proves the efficacy of 3D GS in dealing with scene reconstruction and rendering.

5.3 Performance Benchmarking: Rendering in Dynamic Scenes

This section focuses on the rendering quality in dynamic scenes.

- **Dataset:** The D-NeRF [69] dataset includes videos with 50 to 200 frames each, captured from unique viewpoints. It features synthetic, animated objects in complex scenes, with non-Lambertian materials. The dataset provides 50 to 200 training images and 20 test images per scene, all in 800 × 800 resolution, designed for evaluating models in monocular settings with varied camera poses.

TABLE 4

Quantitative rendering results (§5.4) on nuScenes [147], in terms of PSNR, SSIM, and LPIPS. * denotes numbers taken from [157].

Method	3D GS	PSNR↑	SSIM↑	LPIPS↓
Mip-NeRF [164] [ICCV21]		18.08	0.57	0.55
Mip-NeRF 360 [13] [CVPR22]		22.61	0.69	0.40
Instant-NGP [14] [TOG22]		16.78	0.52	0.57
Urban-NeRF [165] [CVPR22]		20.75	0.63	0.48
S-NeRF [166] [ICLR23]		25.43	0.73	0.30
SUDS [167] [CVPR23]		21.26	0.60	0.47
3D GS* [3] [TOG23]	✓	26.08	0.72	0.30
DrivingGaussian-S [157] [arXiv]	✓	28.36	0.85	0.26
DrivingGaussian-L [157] [arXiv]	✓	28.74	0.86	0.24

- **Benchmarking Algorithms:** For performance comparison, we involve four recent papers which model dynamic scene with 3D GS (*i.e.*, CoGS [84], 4D-GS [73], GauFRé [76], and 4DGS [75]), as well as six NeRF based approaches (*i.e.*, D-NeRF [69], TiNeuVox [159], KPlanes [36], HexPlane-Slim [160], FFDNeRF [72], and MSTH [161]).

- **Evaluation Metric:** PSNR, SSIM [162], and LPIPS [163] are used for measuring RGB rendering performance.

- **Result:** From Table 3 we can observe that 3D GS based methods outperforms existing SOTAs by a clear margin. The static version of 3D GS [3] fails to reconstruct dynamic scenes, resulting in a sharp drop in performance. By modeling the dynamics, CoGS [84] outperforms the SOTA method, FFDNeRF [72], by 5.22dB in terms of PSNR.

5.4 Performance Benchmarking: Rendering in Driving Scenes

This section focuses on the rendering quality in driving scenes.

- **Dataset:** The nuScenes [147] dataset is a comprehensive collection for autonomous driving research, featuring 1000 driving scenes captured using an array of sensors including six cameras, one LiDAR, five RADARs, GPS, and IMU. It provides detailed annotations for 23 object classes with 3D bounding boxes. Six challenging scenes are used for evaluation [157].

TABLE 5

Quantitative avatar modeling results (§5.5) on ZJU-MoCap [168], in terms of PSNR, SSIM, and LPIPS*. The numbers of non-3D GS methods are taken from [110]. The numbers of FPS are taken from [128]. † denotes the average of the values reported in the original paper.

Method	3D GS	PSNR↑	SSIM↑	LPIPS*↓	FPS
NeuralBody [168] [CvPR21]		29.03	0.96	42.47	3.5
AnimNeRF [169] [ICCV21]		29.77	0.96	46.89	2.1
PixelNeRF [170] [ICCV21]		24.71	0.89	121.86	-
NHP [171] [NeurIPS21]		28.25	0.95	64.77	-
HumanNeRF [172] [CvPR22]		30.66	0.97	33.38	0.36
Instant-NVR [173] [CvPR23]		31.01	0.97	38.45	1.53
GART [110] [arXiv]	✓	32.22	0.98	29.21	-
Human101 [128] [arXiv]	✓	31.79	0.96	35.75	104
HUGS† [112] [arXiv]	✓	30.98	0.97	26.67	-
3DGS-Avatar† [125] [arXiv]	✓	30.61	0.97	29.58	-

• **Benchmarking Algorithms:** For performance comparison, we involve one recent paper which models driving scene with 3D GS (*i.e.*, DrivingGaussian [157]), as well as six NeRF based approaches (*i.e.*, Mip-NeRF [164], Mip-NeRF 360 [13], Instant-NGP [14], Urban-NeRF [165], S-NeRF [166], and SUDS [167]).

• **Evaluation Metric:** PSNR, SSIM [162], and LPIPS [163] are used for measuring RGB rendering performance.

• **Result:** The results in Table 4 demonstrate that the 3D GS based methods significantly surpasses the NeRF based methods across all evaluated metrics. For instance, DrivingGaussian-L [157] outperforms S-NeRF [166] by 3.31dB in terms of PSNR. This suggests the great potential of 3D GS for scene representation in autonomous driving.

5.5 Performance Benchmarking: Human Avatar

Human avatar modeling aims to create the model of human avatar from a given multi-view video.

• **Dataset:** ZJU-MoCap [168] dataset is a prevalent benchmark in human modeling from videos, captured with 23 synchronized cameras at a 1024×1024 resolution. Following [172], six subjects (*i.e.*, 377, 386, 387, 392, 393, and 394) are used for evaluation.

• **Benchmarking Algorithms:** For performance comparison, we involve four recent papers which model human avatar with 3D GS (*i.e.*, GART [110], Human101 [128], HUGS [112], and 3DGS-Avatar [125]), as well as six human rendering approaches (*i.e.*, NeuralBody [168], AnimNeRF [169], PixelNeRF [170], NHP [171], HumanNeRF [172], and Instant-NVR [173]).

• **Evaluation Metric:** PSNR, SSIM [162], and LPIPS* [163] are used for measuring RGB rendering performance. Here LPIPS* equals to LPIPS × 1000.

• **Result:** Table 5 presents the numerical results of top-leading solutions in human avatar modeling. We observe that 3D GS based methods demonstrate better performance in both rendering quality and speed. For instance, GART [110] outperforms current SOTA, Instant-NVR [173], by 1.21dB in terms of PSNR. Note that Human101 [128] is about 68 times faster in achieving very competitive accuracy compared to Instant-NVR [173]. These impressive results suggest the power of combining 3D GS with AIGC.

6 FUTURE RESEARCH DIRECTIONS

While recent months have witnessed remarkable follow-up works of 3D GS, there still exist several open challenges that we believe should be overcome.

• **Data-Efficient 3D GS Solutions.** The generation of novel views and the reconstruction of scenes from limited data points are of significant interest, particularly for their potential to enhance realism and user experience with minimal input. Recent advances have explored the use of depth information [174]–[176], dense probability distributions [177], and pixel-to-Gaussian mapping [178] to facilitate this capability. However, there remains an urgent need for further exploration in this domain. In addition, a notable issue of 3D GS is the emergence of artifacts in areas with insufficient observational data. This challenge is a prevalent limitation in radiance field rendering, where sparse data often leads to inaccuracies in reconstruction. Consequently, the development of novel methods for data interpolation or integration in these sparse regions represents a promising avenue for future research.

• **Memory-Efficient 3D GS Solutions.** While 3D GS demonstrates remarkable capabilities, its scalability poses significant challenges, particularly when juxtaposed with NeRF-based methods. The latter benefits from the simplicity of storing merely the parameters of a learned MLP. This scalability issue becomes increasingly acute in the context of large-scale scene management, where the computational and memory demands escalate substantially. Consequently, there is an urgent need to optimize memory utilization during both the training phase and in the storage of the model. Exploring more efficient data structures and investigating advanced compression techniques represent promising avenues to address these limitations [179]–[182].

• **Advanced Rendering Algorithms.** The current rendering pipeline of 3D GS is straightforward and can be further optimized. For instance, the simple visibility algorithm may lead to cause a drastic switch in depth/blending order of Gaussians. This underscores a significant opportunity for future research: the implementation of more advanced rendering algorithms. These improved methodologies should aim to more accurately simulate the intricate interplay of light and material properties [183], [184] within a given scene. A promising approach could involve the assimilation and adaptation of established principles from traditional computer graphics into the specific context of 3D GS. Noteworthy in this regard is the ongoing effort to integrate enhanced rendering techniques [185]–[188], or hybrid models [189], into current computational frameworks of 3D GS. Furthermore, the exploration of inverse rendering and its applications [190], [191] presents a fertile ground for investigation.

• **Optimization and Regularization.** The anisotropic Gaussians, while beneficial for representing complex geometries, can create undesirable visual artifacts. For example, those large 3D Gaussians, especially in regions with view-dependent appearance, can cause popping artifacts, where visual elements abruptly appear or disappear, breaking the immersion. There is considerable potential for exploration in the regularization and optimization of 3D GS. Introducing antialiasing could mitigate the abrupt changes in depth and

blending order of Gaussians. Enhancements in optimization algorithms might better control Gaussians in space and beyond [192], [193]. Further, incorporating regularization into the optimization process may accelerate convergence, smooth visual noise, or improve image quality [176]. In addition, as mentioned in Sec. 3.2, such a large number of hyperparameters affects the generalization of 3D GS, which is in dire need of a solution.

• **3D Gaussians in Mesh Reconstruction.** The potential of 3D GS in mesh reconstruction and its position in the spectrum of volumetric and surface representations is yet to be fully explored. Researching how Gaussian primitives can be adapted for mesh reconstruction tasks is urgently needed. This exploration could bridge the gap between volumetric rendering and traditional surface-based methods, offering insights into new rendering techniques and applications. There are some early explorations [194]–[196] about mesh extraction and reconstruction based on 3D Gaussians.

• **Empowering 3D GS with More Possibilities.** Despite the significant potential of 3D GS, the full scope of applications for 3D GS remains largely untapped. A promising avenue for exploration involves augmenting 3D Gaussians with additional attributes, such as linguistic [197]–[199] and physical [200], [201] properties, tailored for specific applications. Moreover, recent studies have begun to unveil the capability of 3D GS in several domains, *e.g.*, camera pose estimation [202], the capture of hand-object interactions [203], and the quantification of uncertainty [204]. These preliminary findings highlight a significant opportunity for interdisciplinary scholars to explore 3D GS further.

7 CONCLUSIONS

To the best of our knowledge, this survey presents the first comprehensive overview of 3D GS, a groundbreaking technique revolutionizing explicit radiance fields and computer graphics. It delineates the paradigm shift from traditional NeRF methodologies, spotlighting the advantages of 3D GS in real-time rendering and enhanced controllability. Our detailed analysis demonstrates the superiority of 3D GS in practical applications, particularly those necessitating real-time performance. We offer insights into prospective research directions and the unresolved challenges within this domain. Overall, 3D GS stands as a transformative technology, poised to significantly influence future advancements in 3D reconstruction and representation. This survey is intended to serve as a foundational resource, propelling further exploration and progress in this rapidly evolving field.

REFERENCES

- [1] B. Mildenhall, P. P. Srinivasan, M. Tancik, J. T. Barron, R. Ramamoorthi, and R. Ng, "Nerf: Representing scenes as neural radiance fields for view synthesis," in *Proc. Eur. Conf. Comput. Vis.* Springer, 2020, pp. 405–421.
- [2] S. Avidan and A. Shashua, "Novel view synthesis in tensor space," in *Proc. IEEE Conf. Comput. Vis. Pattern Recognit.*, 1997, pp. 1034–1040.
- [3] B. Kerbl, G. Kopanas, T. Leimkühler, and G. Drettakis, "3d gaussian splatting for real-time radiance field rendering," *ACM Tran. Graphics*, vol. 42, no. 4, 2023.
- [4] S. J. Gortler, R. Grzeszczuk, R. Szeliski, and M. F. Cohen, "The lumigraph," in *Seminal Graphics Papers: Pushing the Boundaries, Volume 2*, 2023, pp. 453–464.
- [5] M. Levoy and P. Hanrahan, "Light field rendering," in *Seminal Graphics Papers: Pushing the Boundaries, Volume 2*, 2023, pp. 441–452.
- [6] C. Buehler, M. Bosse, L. McMillan, S. Gortler, and M. Cohen, "Unstructured lumigraph rendering," in *Seminal Graphics Papers: Pushing the Boundaries, Volume 2*, 2023, pp. 497–504.
- [7] N. Snavely, S. M. Seitz, and R. Szeliski, "Photo tourism: exploring photo collections in 3d," in *ACM Tran. Graphics*, 2006, pp. 835–846.
- [8] M. Goesele, N. Snavely, B. Curless, H. Hoppe, and S. M. Seitz, "Multi-view stereo for community photo collections," in *Proc. IEEE Int. Conf. Comput. Vis.* IEEE, 2007, pp. 1–8.
- [9] A. Chen, Z. Xu, A. Geiger, J. Yu, and H. Su, "Tensorf: Tensorial radiance fields," in *European Conference on Computer Vision*. Springer, 2022, pp. 333–350.
- [10] S. J. Garbin, M. Kowalski, M. Johnson, J. Shotton, and J. Valentin, "Fastnerf: High-fidelity neural rendering at 200fps," in *Proceedings of the IEEE/CVF International Conference on Computer Vision*, 2021, pp. 14 346–14 355.
- [11] C. Reiser, S. Peng, Y. Liao, and A. Geiger, "Kilonerf: Speeding up neural radiance fields with thousands of tiny mlps," in *Proceedings of the IEEE/CVF International Conference on Computer Vision*, 2021, pp. 14 335–14 345.
- [12] T. Takikawa, J. Litalien, K. Yin, K. Kreis, C. Loop, D. Nowrouzezahrai, A. Jacobson, M. McGuire, and S. Fidler, "Neural geometric level of detail: Real-time rendering with implicit 3d shapes," in *Proceedings of the IEEE/CVF Conference on Computer Vision and Pattern Recognition*, 2021, pp. 11 358–11 367.
- [13] J. T. Barron, B. Mildenhall, D. Verbin, P. P. Srinivasan, and P. Hedman, "Mip-nerf 360: Unbounded anti-aliased neural radiance fields," in *Proceedings of the IEEE/CVF Conference on Computer Vision and Pattern Recognition*, 2022, pp. 5470–5479.
- [14] T. Müller, A. Evans, C. Schied, and A. Keller, "Instant neural graphics primitives with a multiresolution hash encoding," *ACM Transactions on Graphics (ToG)*, vol. 41, no. 4, pp. 1–15, 2022.
- [15] P. Henzler, N. J. Mitra, and T. Ritschel, "Escaping plato's cave: 3d shape from adversarial rendering," in *Proc. IEEE Int. Conf. Comput. Vis.*, 2019, pp. 9984–9993.
- [16] V. Sitzmann, J. Thies, F. Heide, M. Nießner, G. Wetzstein, and M. Zollhofer, "Deepvoxels: Learning persistent 3d feature embeddings," in *Proc. IEEE Conf. Comput. Vis. Pattern Recognit.*, 2019, pp. 2437–2446.
- [17] H. Pfister, M. Zwicker, J. Van Baar, and M. Gross, "Surfels: Surface elements as rendering primitives," in *Proceedings of the 27th annual conference on Computer graphics and interactive techniques*, 2000, pp. 335–342.
- [18] M. Zwicker, H. Pfister, J. Van Baar, and M. Gross, "Surface splatting," in *Proceedings of the 28th annual conference on Computer graphics and interactive techniques*, 2001, pp. 371–378.
- [19] L. Ren, H. Pfister, and M. Zwicker, "Object space ewa surface splatting: A hardware accelerated approach to high quality point rendering," in *Computer Graphics Forum*, vol. 21, no. 3. Wiley Online Library, 2002, pp. 461–470.
- [20] M. Botsch, A. Hornung, M. Zwicker, and L. Kobbelt, "High-quality surface splatting on today's gpus," in *Proceedings Eurographics/IEEE VGTC Symposium Point-Based Graphics*, 2005. IEEE, 2005, pp. 17–141.
- [21] W. Yifan, F. Serena, S. Wu, C. Öztireli, and O. Sorkine-Hornung, "Differentiable surface splatting for point-based geometry processing," *ACM Transactions on Graphics (TOG)*, vol. 38, no. 6, pp. 1–14, 2019.
- [22] O. Wiles, G. Gkioxari, R. Szeliski, and J. Johnson, "Synsin: End-to-end view synthesis from a single image," in *Proceedings of the IEEE/CVF Conference on Computer Vision and Pattern Recognition*, 2020, pp. 7467–7477.
- [23] D. Kalkofen, E. Mendez, and D. Schmalstieg, "Comprehensible visualization for augmented reality," *IEEE Trans. Vis. Comput. Graphics*, vol. 15, no. 2, pp. 193–204, 2008.
- [24] A. Patney, M. Salvi, J. Kim, A. Kaplanyan, C. Wyman, N. Bentley, D. Luebke, and A. Lefohn, "Towards foveated rendering for gaze-tracked virtual reality," *ACM Transactions on Graphics (TOG)*, vol. 35, no. 6, pp. 1–12, 2016.

- [25] R. Albert, A. Patney, D. Luebke, and J. Kim, "Latency requirements for foveated rendering in virtual reality," *ACM Transactions on Applied Perception (TAP)*, vol. 14, no. 4, pp. 1–13, 2017.
- [26] R. Chabra, J. E. Lenssen, E. Ilg, T. Schmidt, J. Straub, S. Lovegrove, and R. Newcombe, "Deep local shapes: Learning local sdf priors for detailed 3d reconstruction," in *Proc. Eur. Conf. Comput. Vis.* Springer, 2020, pp. 608–625.
- [27] Z. Wang, J. Phillion, S. Fidler, and J. Kautz, "Learning indoor inverse rendering with 3d spatially-varying lighting," in *Proceedings of the IEEE/CVF International Conference on Computer Vision*, 2021, pp. 12 538–12 547.
- [28] C. Sun, M. Sun, and H.-T. Chen, "Direct voxel grid optimization: Super-fast convergence for radiance fields reconstruction," in *Proceedings of the IEEE/CVF Conference on Computer Vision and Pattern Recognition*, 2022, pp. 5459–5469.
- [29] L. Kobbelt and M. Botsch, "A survey of point-based techniques in computer graphics," *Computers & Graphics*, vol. 28, no. 6, pp. 801–814, 2004.
- [30] Y. Xie, T. Takikawa, S. Saito, O. Litany, S. Yan, N. Khan, F. Tombari, J. Tompkin, V. Sitzmann, and S. Sridhar, "Neural fields in visual computing and beyond," in *Computer Graphics Forum*, vol. 41, no. 2. Wiley Online Library, 2022, pp. 641–676.
- [31] A. Tewari, J. Thies, B. Mildenhall, P. Srinivasan, E. Treitsch, W. Yifan, C. Lassner, V. Sitzmann, R. Martin-Brualla, S. Lombardi *et al.*, "Advances in neural rendering," in *Computer Graphics Forum*, vol. 41, no. 2. Wiley Online Library, 2022, pp. 703–735.
- [32] X.-F. Han, H. Laga, and M. Bannamoun, "Image-based 3d object reconstruction: State-of-the-art and trends in the deep learning era," *IEEE Trans. Pattern Anal. Mach. Intell.*, vol. 43, no. 5, pp. 1578–1604, 2019.
- [33] J. Yuan, T. Chen, B. Li, and X. Xue, "Compositional scene representation learning via reconstruction: A survey," *IEEE Trans. Pattern Anal. Mach. Intell.*, 2023.
- [34] L. Mescheder, M. Oechsle, M. Niemeyer, S. Nowozin, and A. Geiger, "Occupancy networks: Learning 3d reconstruction in function space," in *Proceedings of the IEEE/CVF conference on computer vision and pattern recognition*, 2019, pp. 4460–4470.
- [35] J. J. Park, P. Florence, J. Straub, R. Newcombe, and S. Lovegrove, "DeepSDF: Learning continuous signed distance functions for shape representation," in *Proceedings of the IEEE/CVF conference on computer vision and pattern recognition*, 2019, pp. 165–174.
- [36] S. Fridovich-Keil, G. Meanti, F. R. Warburg, B. Recht, and A. Kanazawa, "K-planes: Explicit radiance fields in space, time, and appearance," in *Proceedings of the IEEE/CVF Conference on Computer Vision and Pattern Recognition*, 2023, pp. 12 479–12 488.
- [37] M. Eisemann, B. De Decker, M. Magnor, P. Bekaert, E. De Aguiar, N. Ahmed, C. Theobalt, and A. Sellent, "Floating textures," in *Computer graphics forum*, vol. 27, no. 2. Wiley Online Library, 2008, pp. 409–418.
- [38] G. Chaurasia, S. Duchene, O. Sorkine-Hornung, and G. Drettakis, "Depth synthesis and local warps for plausible image-based navigation," *ACM Tran. Graphics*, vol. 32, no. 3, pp. 1–12, 2013.
- [39] P. Hedman, J. Philip, T. Price, J.-M. Frahm, G. Drettakis, and G. Brostow, "Deep blending for free-viewpoint image-based rendering," *ACM Tran. Graphics*, vol. 37, no. 6, pp. 1–15, 2018.
- [40] G. Kopanas, J. Philip, T. Leimkühler, and G. Drettakis, "Point-based neural rendering with per-view optimization," in *Computer Graphics Forum*, vol. 40, no. 4. Wiley Online Library, 2021, pp. 29–43.
- [41] J. Flynn, I. Neulander, J. Philbin, and N. Snavely, "Deepstereo: Learning to predict new views from the world's imagery," in *Proc. IEEE Conf. Comput. Vis. Pattern Recognit.*, 2016, pp. 5515–5524.
- [42] T. Zhou, S. Tulsiani, W. Sun, J. Malik, and A. A. Efros, "View synthesis by appearance flow," in *Proc. Eur. Conf. Comput. Vis.* Springer, 2016, pp. 286–301.
- [43] J. Thies, M. Zollhöfer, and M. Nießner, "Deferred neural rendering: Image synthesis using neural textures," *ACM Tran. Graphics*, vol. 38, no. 4, pp. 1–12, 2019.
- [44] G. Riegler and V. Koltun, "Free view synthesis," in *Proc. Eur. Conf. Comput. Vis.* Springer, 2020, pp. 623–640.
- [45] E. Penner and L. Zhang, "Soft 3d reconstruction for view synthesis," *ACM Tran. Graphics*, vol. 36, no. 6, pp. 1–11, 2017.
- [46] K.-A. Aliev, A. Sevastopolsky, M. Kolos, D. Ulyanov, and V. Lempitsky, "Neural point-based graphics," in *Proc. Eur. Conf. Comput. Vis.* Springer, 2020, pp. 696–712.
- [47] D. Rückert, L. Franke, and M. Stamminger, "Adop: Approximate differentiable one-pixel point rendering," *ACM Tran. Graphics*, vol. 41, no. 4, pp. 1–14, 2022.
- [48] S. Laine and T. Karras, "High-performance software rasterization on gpus," in *Proceedings of the ACM SIGGRAPH Symposium on High Performance Graphics*, 2011, pp. 79–88.
- [49] M. Schütz, B. Kerbl, and M. Wimmer, "Software rasterization of 2 billion points in real time," *Proceedings of the ACM on Computer Graphics and Interactive Techniques*, vol. 5, no. 3, pp. 1–17, 2022.
- [50] M. Zwicker, H. Pfister, J. Van Baar, and M. Gross, "Ewa volume splatting," in *Proceedings Visualization, 2001. VIS'01.* IEEE, 2001, pp. 29–538.
- [51] J. A. Placed, J. Strader, H. Carrillo, N. Atanasov, V. Indelman, L. Carlone, and J. A. Castellanos, "A survey on active simultaneous localization and mapping: State of the art and new frontiers," *IEEE Transactions on Robotics*, 2023.
- [52] H. Durrant-Whyte and T. Bailey, "Simultaneous localization and mapping: part i," *IEEE robotics & automation magazine*, vol. 13, no. 2, pp. 99–110, 2006.
- [53] T. Bailey and H. Durrant-Whyte, "Simultaneous localization and mapping (slam): Part ii," *IEEE robotics & automation magazine*, vol. 13, no. 3, pp. 108–117, 2006.
- [54] R. A. Newcombe, S. Izadi, O. Hilliges, D. Molyneaux, D. Kim, A. J. Davison, P. Kohi, J. Shotton, S. Hodges, and A. Fitzgibbon, "Kinectfusion: Real-time dense surface mapping and tracking," in *2011 10th IEEE international symposium on mixed and augmented reality*. Ieee, 2011, pp. 127–136.
- [55] M. Nießner, M. Zollhöfer, S. Izadi, and M. Stamminger, "Real-time 3d reconstruction at scale using voxel hashing," *ACM Transactions on Graphics (ToG)*, vol. 32, no. 6, pp. 1–11, 2013.
- [56] R. Maier, R. Schaller, and D. Cremers, "Efficient online surface correction for real-time large-scale 3d reconstruction," *arXiv preprint arXiv:1709.03763*, 2017.
- [57] O. Kähler, V. Prisacariu, J. Valentin, and D. Murray, "Hierarchical voxel block hashing for efficient integration of depth images," *IEEE Robotics and Automation Letters*, vol. 1, no. 1, pp. 192–197, 2015.
- [58] F. Ruetz, E. Hernández, M. Pfeiffer, H. Oleynikova, M. Cox, T. Lowe, and P. Borges, "Ovpc mesh: 3d free-space representation for local ground vehicle navigation," in *2019 International Conference on Robotics and Automation (ICRA)*. IEEE, 2019, pp. 8648–8654.
- [59] T. Whelan, R. F. Salas-Moreno, B. Glocker, A. J. Davison, and S. Leutenegger, "Elasticfusion: Real-time dense slam and light source estimation," *The International Journal of Robotics Research*, vol. 35, no. 14, pp. 1697–1716, 2016.
- [60] K. Wang, F. Gao, and S. Shen, "Real-time scalable dense surfel mapping," in *2019 International conference on robotics and automation (ICRA)*. IEEE, 2019, pp. 6919–6925.
- [61] R. Mur-Artal and J. D. Tardós, "Orb-slam2: An open-source slam system for monocular, stereo, and rgb-d cameras," *IEEE transactions on robotics*, vol. 33, no. 5, pp. 1255–1262, 2017.
- [62] H. Huang, L. Li, H. Cheng, and S.-K. Yeung, "Photo-slam: Real-time simultaneous localization and photorealistic mapping for monocular, stereo, and rgb-d cameras," *arXiv preprint arXiv:2311.16728*, 2023.
- [63] H. Matsuki, R. Murai, P. H. Kelly, and A. J. Davison, "Gaussian splatting slam," *arXiv preprint arXiv:2312.06741*, 2023.
- [64] V. Yugay, Y. Li, T. Gevers, and M. R. Oswald, "Gaussian-slam: Photo-realistic dense slam with gaussian splatting," *arXiv preprint arXiv:2312.10070*, 2023.
- [65] C. Yan, D. Qu, D. Wang, D. Xu, Z. Wang, B. Zhao, and X. Li, "Gs-slam: Dense visual slam with 3d gaussian splatting," *arXiv preprint arXiv:2311.11700*, 2023.
- [66] N. Keetha, J. Karhade, K. M. Jatavallabhula, G. Yang, S. Scherer, D. Ramanan, and J. Luiten, "Splatam: Splat, track & map 3d gaussians for dense rgb-d slam," *arXiv preprint arXiv:2312.02126*, 2023.
- [67] Y. Chen, C. Gu, J. Jiang, X. Zhu, and L. Zhang, "Periodic vibration gaussian: Dynamic urban scene reconstruction and real-time rendering," *arXiv preprint arXiv:2311.18561*, 2023.
- [68] Y. Yan, H. Lin, C. Zhou, W. Wang, H. Sun, K. Zhan, X. Lang, X. Zhou, and S. Peng, "Street gaussians for modeling dynamic urban scenes," *arXiv preprint arXiv:2401.01339*, 2024.
- [69] A. Pumarola, E. Corona, G. Pons-Moll, and F. Moreno-Noguer, "D-nerf: Neural radiance fields for dynamic scenes," in *Proceed-*

- ings of the *IEEE/CVF Conference on Computer Vision and Pattern Recognition*, 2021, pp. 10318–10327.
- [70] K. Park, U. Sinha, P. Hedman, J. T. Barron, S. Bouaziz, D. B. Goldman, R. Martin-Brualla, and S. M. Seitz, “Hypernerf: A higher-dimensional representation for topologically varying neural radiance fields,” *arXiv preprint arXiv:2106.13228*, 2021.
- [71] K. Park, U. Sinha, J. T. Barron, S. Bouaziz, D. B. Goldman, S. M. Seitz, and R. Martin-Brualla, “Nerfies: Deformable neural radiance fields,” in *Proceedings of the IEEE/CVF International Conference on Computer Vision*, 2021, pp. 5865–5874.
- [72] X. Guo, J. Sun, Y. Dai, G. Chen, X. Ye, X. Tan, E. Ding, Y. Zhang, and J. Wang, “Forward flow for novel view synthesis of dynamic scenes,” in *Proceedings of the IEEE/CVF International Conference on Computer Vision*, 2023, pp. 16 022–16 033.
- [73] G. Wu, T. Yi, J. Fang, L. Xie, X. Zhang, W. Wei, W. Liu, Q. Tian, and X. Wang, “4d gaussian splatting for real-time dynamic scene rendering,” *arXiv preprint arXiv:2310.08528*, 2023.
- [74] J. Luiten, G. Kopanas, B. Leibe, and D. Ramanan, “Dynamic 3d gaussians: Tracking by persistent dynamic view synthesis,” *arXiv preprint arXiv:2308.09713*, 2023.
- [75] Z. Yang, H. Yang, Z. Pan, X. Zhu, and L. Zhang, “Real-time photorealistic dynamic scene representation and rendering with 4d gaussian splatting,” *arXiv preprint arXiv:2310.10642*, 2023.
- [76] Y. Liang, N. Khan, Z. Li, T. Nguyen-Phuoc, D. Lanman, J. Tompkin, and L. Xiao, “Gaufre: Gaussian deformation fields for real-time dynamic novel view synthesis,” *arXiv preprint arXiv:2312.11458*, 2023.
- [77] Y. Lin, Z. Dai, S. Zhu, and Y. Yao, “Gaussian-flow: 4d reconstruction with dynamic 3d gaussian particle,” *arXiv preprint arXiv:2312.03431*, 2023.
- [78] Z. Yang, X. Gao, W. Zhou, S. Jiao, Y. Zhang, and X. Jin, “Deformable 3d gaussians for high-fidelity monocular dynamic scene reconstruction,” *arXiv preprint arXiv:2309.13101*, 2023.
- [79] A. Kratimenos, J. Lei, and K. Daniilidis, “Dyngmf: Neural motion factorization for real-time dynamic view synthesis with 3d gaussian splatting,” *arXiv preprint arXiv:2312.00112*, 2023.
- [80] D. Das, C. Wewer, R. Yunus, E. Ilg, and J. E. Lenssen, “Neural parametric gaussians for monocular non-rigid object reconstruction,” *arXiv preprint arXiv:2312.01196*, 2023.
- [81] R. Shaw, J. Song, A. Moreau, M. Nazarczuk, S. Catley-Chandar, H. Dharmo, and E. Perez-Pellitero, “Swags: Sampling windows adaptively for dynamic 3d gaussian splatting,” *arXiv preprint arXiv:2312.13308*, 2023.
- [82] Y.-H. Huang, Y.-T. Sun, Z. Yang, X. Lyu, Y.-P. Cao, and X. Qi, “Sc-gs: Sparse-controlled gaussian splatting for editable dynamic scenes,” *arXiv preprint arXiv:2312.14937*, 2023.
- [83] R. Shao, J. Sun, C. Peng, Z. Zheng, B. Zhou, H. Zhang, and Y. Liu, “Control4d: Dynamic portrait editing by learning 4d gan from 2d diffusion-based editor,” *arXiv preprint arXiv:2305.20082*, 2023.
- [84] H. Yu, J. Julin, Z. Á. Milacski, K. Niinuma, and L. A. Jeni, “Cogs: Controllable gaussian splatting,” *arXiv preprint arXiv:2312.05664*, 2023.
- [85] K. Katsumata, D. M. Vo, and H. Nakayama, “An efficient 3d gaussian representation for monocular/multi-view dynamic scenes,” *arXiv preprint arXiv:2311.12897*, 2023.
- [86] Z. Li, Z. Chen, Z. Li, and Y. Xu, “Spacetime gaussian feature splatting for real-time dynamic view synthesis,” *arXiv preprint arXiv:2312.16812*, 2023.
- [87] I. Goodfellow, J. Pouget-Abadie, M. Mirza, B. Xu, D. Warde-Farley, S. Ozair, A. Courville, and Y. Bengio, “Generative adversarial networks,” *Communications of the ACM*, vol. 63, no. 11, pp. 139–144, 2020.
- [88] J. Ho, A. Jain, and P. Abbeel, “Denoising diffusion probabilistic models,” *Advances in neural information processing systems*, vol. 33, pp. 6840–6851, 2020.
- [89] L. Zhang, A. Rao, and M. Agrawala, “Adding conditional control to text-to-image diffusion models,” in *Proceedings of the IEEE/CVF International Conference on Computer Vision*, 2023, pp. 3836–3847.
- [90] R. Rombach, A. Blattmann, D. Lorenz, P. Esser, and B. Ommer, “High-resolution image synthesis with latent diffusion models,” in *Proceedings of the IEEE/CVF conference on computer vision and pattern recognition*, 2022, pp. 10 684–10 695.
- [91] Z. Chen, F. Wang, and H. Liu, “Text-to-3d using gaussian splatting,” *arXiv preprint arXiv:2309.16585*, 2023.
- [92] J. Tang, J. Ren, H. Zhou, Z. Liu, and G. Zeng, “Dreamgaussian: Generative gaussian splatting for efficient 3d content creation,” *arXiv preprint arXiv:2309.16653*, 2023.
- [93] T. Yi, J. Fang, G. Wu, L. Xie, X. Zhang, W. Liu, Q. Tian, and X. Wang, “Gaussiandreamer: Fast generation from text to 3d gaussian splatting with point cloud priors,” *arXiv preprint arXiv:2310.08529*, 2023.
- [94] X. Li, H. Wang, and K.-K. Tseng, “Gaussiandiffusion: 3d gaussian splatting for denoising diffusion probabilistic models with structured noise,” *arXiv preprint arXiv:2311.11221*, 2023.
- [95] Y. Liang, X. Yang, J. Lin, H. Li, X. Xu, and Y. Chen, “Lucidreamer: Towards high-fidelity text-to-3d generation via interval score matching,” *arXiv preprint arXiv:2311.11284*, 2023.
- [96] J. Chung, S. Lee, H. Nam, J. Lee, and K. M. Lee, “Luciddreamer: Domain-free generation of 3d gaussian splatting scenes,” *arXiv preprint arXiv:2311.13384*, 2023.
- [97] X. Liu, X. Zhan, J. Tang, Y. Shan, G. Zeng, D. Lin, X. Liu, and Z. Liu, “Humangaussian: Text-driven 3d human generation with gaussian splatting,” *arXiv preprint arXiv:2311.17061*, 2023.
- [98] A. Vilesov, P. Chari, and A. Kadambi, “Cg3d: Compositional generation for text-to-3d via gaussian splatting,” *arXiv preprint arXiv:2311.17907*, 2023.
- [99] X. Yang, Y. Chen, C. Chen, C. Zhang, Y. Xu, X. Yang, F. Liu, and G. Lin, “Learn to optimize denoising scores for 3d generation: A unified and improved diffusion prior on nerf and 3d gaussian splatting,” *arXiv preprint arXiv:2312.04820*, 2023.
- [100] Z.-X. Zou, Z. Yu, Y.-C. Guo, Y. Li, D. Liang, Y.-P. Cao, and S.-H. Zhang, “Triplane meets gaussian splatting: Fast and generalizable single-view 3d reconstruction with transformers,” *arXiv preprint arXiv:2312.09147*, 2023.
- [101] H. Ling, S. W. Kim, A. Torralba, S. Fidler, and K. Kreis, “Align your gaussians: Text-to-4d with dynamic 3d gaussians and composed diffusion models,” *arXiv preprint arXiv:2312.13763*, 2023.
- [102] J. Ren, L. Pan, J. Tang, C. Zhang, A. Cao, G. Zeng, and Z. Liu, “Dreamgaussian4d: Generative 4d gaussian splatting,” *arXiv preprint arXiv:2312.17142*, 2023.
- [103] Y. Yin, D. Xu, Z. Wang, Y. Zhao, and Y. Wei, “4dgen: Grounded 4d content generation with spatial-temporal consistency,” *arXiv preprint arXiv:2312.17225*, 2023.
- [104] H. Ouyang, K. Heal, S. Lombardi, and T. Sun, “Text2immersion: Generative immersive scene with 3d gaussians,” *arXiv preprint arXiv:2312.09242*, 2023.
- [105] J. Zhang, Z. Tang, Y. Pang, X. Cheng, P. Jin, Y. Wei, W. Yu, M. Ning, and L. Yuan, “Repaint123: Fast and high-quality one image to 3d generation with progressive controllable 2d repainting,” *arXiv preprint arXiv:2312.13271*, 2023.
- [106] W. Zielonka, T. Bagautdinov, S. Saito, M. Zollhöfer, J. Thies, and J. Romero, “Drivable 3d gaussian avatars,” *arXiv preprint arXiv:2311.08581*, 2023.
- [107] R. Jena, G. S. Iyer, S. Choudhary, B. Smith, P. Chaudhari, and J. Gee, “Splatarmor: Articulated gaussian splatting for animatable humans from monocular rgb videos,” *arXiv preprint arXiv:2311.10812*, 2023.
- [108] K. Ye, T. Shao, and K. Zhou, “Animatable 3d gaussians for high-fidelity synthesis of human motions,” *arXiv preprint arXiv:2311.13404*, 2023.
- [109] Z. Li, Z. Zheng, L. Wang, and Y. Liu, “Animatable gaussians: Learning pose-dependent gaussian maps for high-fidelity human avatar modeling,” *arXiv preprint arXiv:2311.16096*, 2023.
- [110] J. Lei, Y. Wang, G. Pavlakos, L. Liu, and K. Daniilidis, “Gart: Gaussian articulated template models,” *arXiv preprint arXiv:2311.16099*, 2023.
- [111] A. Moreau, J. Song, H. Dharmo, R. Shaw, Y. Zhou, and E. Pérez-Pellitero, “Human gaussian splatting: Real-time rendering of animatable avatars,” *arXiv preprint arXiv:2311.17113*, 2023.
- [112] M. Kocabas, J.-H. R. Chang, J. Gabriel, O. Tuzel, and A. Ranjan, “Hugs: Human gaussian splats,” *arXiv preprint arXiv:2311.17910*, 2023.
- [113] R. Abdal, W. Yifan, Z. Shi, Y. Xu, R. Po, Z. Kuang, Q. Chen, D.-Y. Yeung, and G. Wetzstein, “Gaussian shell maps for efficient 3d human generation,” *arXiv preprint arXiv:2311.17857*, 2023.
- [114] J. Wang, X. Li, J. Xie, F. Xu, and H. Gao, “Gaussianhead: Impressive 3d gaussian-based head avatars with dynamic hybrid neural field,” *arXiv preprint arXiv:2312.01632*, 2023.
- [115] S. Qian, T. Kirschstein, L. Schoneveld, D. Davoli, S. Giebenhain, and M. Nießner, “Gaussianavatars: Photorealistic head avatars with rigged 3d gaussians,” *arXiv preprint arXiv:2312.02069*, 2023.
- [116] S. Zheng, B. Zhou, R. Shao, B. Liu, S. Zhang, L. Nie, and Y. Liu, “Gps-gaussian: Generalizable pixel-wise 3d gaussian

- splatting for real-time human novel view synthesis," *arXiv preprint arXiv:2312.02155*, 2023.
- [117] S. Hu and Z. Liu, "Gauhuman: Articulated gaussian splatting from monocular human videos," *arXiv preprint arXiv:2312.02973*, 2023.
- [118] H. Dharmo, Y. Nie, A. Moreau, J. Song, R. Shaw, Y. Zhou, and E. Pérez-Pellitero, "Headgas: Real-time animatable head avatars via 3d gaussian splatting," *arXiv preprint arXiv:2312.02902*, 2023.
- [119] Y. Jiang, Z. Shen, P. Wang, Z. Su, Y. Hong, Y. Zhang, J. Yu, and L. Xu, "Hifi4g: High-fidelity human performance rendering via compact gaussian splatting," *arXiv preprint arXiv:2312.03461*, 2023.
- [120] L. Hu, H. Zhang, Y. Zhang, B. Zhou, B. Liu, S. Zhang, and L. Nie, "Gaussianavatar: Towards realistic human avatar modeling from a single video via animatable 3d gaussians," *arXiv preprint arXiv:2312.02134*, 2023.
- [121] J. Xiang, X. Gao, Y. Guo, and J. Zhang, "Flashavatar: High-fidelity digital avatar rendering at 300fps," *arXiv preprint arXiv:2312.02214*, 2023.
- [122] S. Saito, G. Schwartz, T. Simon, J. Li, and G. Nam, "Relightable gaussian codec avatars," *arXiv preprint arXiv:2312.03704*, 2023.
- [123] Y. Chen, L. Wang, Q. Li, H. Xiao, S. Zhang, H. Yao, and Y. Liu, "Monogaussianavatar: Monocular gaussian point-based head avatar," *arXiv preprint arXiv:2312.04558*, 2023.
- [124] H. Pang, H. Zhu, A. Kortylewski, C. Theobalt, and M. Habermann, "Ash: Animatable gaussian splats for efficient and photo-real human rendering," *arXiv preprint arXiv:2312.05941*, 2023.
- [125] Z. Qian, S. Wang, M. Mihajlovic, A. Geiger, and S. Tang, "3dgs-avatar: Animatable avatars via deformable 3d gaussian splatting," *arXiv preprint arXiv:2312.09228*, 2023.
- [126] Y. Yuan, X. Li, Y. Huang, S. De Mello, K. Nagano, J. Kautz, and U. Iqbal, "Gavatar: Animatable 3d gaussian avatars with implicit mesh learning," *arXiv preprint arXiv:2312.11461*, 2023.
- [127] H. Jung, N. Brasch, J. Song, E. Perez-Pellitero, Y. Zhou, Z. Li, N. Navab, and B. Busam, "Deformable 3d gaussian splatting for animatable human avatars," *arXiv preprint arXiv:2312.15059*, 2023.
- [128] M. Li, J. Tao, Z. Yang, and Y. Yang, "Human101: Training 100+ fps human gaussians in 100s from 1 view," *arXiv preprint arXiv:2312.15258*, 2023.
- [129] Y. Chen, Z. Chen, C. Zhang, F. Wang, X. Yang, Y. Wang, Z. Cai, L. Yang, H. Liu, and G. Lin, "Gaussianeditor: Swift and controllable 3d editing with gaussian splatting," *arXiv preprint arXiv:2311.14521*, 2023.
- [130] J. Fang, J. Wang, X. Zhang, L. Xie, and Q. Tian, "Gaussianeditor: Editing 3d gaussians delicately with text instructions," *arXiv preprint arXiv:2311.16037*, 2023.
- [131] J. Huang and H. Yu, "Point'n move: Interactive scene object manipulation on gaussian splatting radiance fields," *arXiv preprint arXiv:2311.16737*, 2023.
- [132] M. Ye, M. Danelljan, F. Yu, and L. Ke, "Gaussian grouping: Segment and edit anything in 3d scenes," *arXiv preprint arXiv:2312.00732*, 2023.
- [133] J. Cen, J. Fang, C. Yang, L. Xie, X. Zhang, W. Shen, and Q. Tian, "Segment any 3d gaussians," *arXiv preprint arXiv:2312.00860*, 2023.
- [134] S. Zhou, H. Chang, S. Jiang, Z. Fan, Z. Zhu, D. Xu, P. Chari, S. You, Z. Wang, and A. Kadambi, "Feature 3dgs: Supercharging 3d gaussian splatting to enable distilled feature fields," *arXiv preprint arXiv:2312.03203*, 2023.
- [135] K. Lan, H. Li, H. Shi, W. Wu, Y. Liao, L. Wang, and P. Zhou, "2d-guided 3d gaussian segmentation," *arXiv preprint arXiv:2312.16047*, 2023.
- [136] J. Straub, T. Whelan, L. Ma, Y. Chen, E. Wijmans, S. Green, J. J. Engel, R. Mur-Artal, C. Ren, S. Verma *et al.*, "The replica dataset: A digital replica of indoor spaces," *arXiv preprint arXiv:1906.05797*, 2019.
- [137] J. Park, Q.-Y. Zhou, and V. Koltun, "Colored point cloud registration revisited," in *Proceedings of the IEEE international conference on computer vision*, 2017, pp. 143–152.
- [138] E. Sucar, S. Liu, J. Ortiz, and A. J. Davison, "imap: Implicit mapping and positioning in real-time," in *Proceedings of the IEEE/CVF International Conference on Computer Vision*, 2021, pp. 6229–6238.
- [139] X. Yang, H. Li, H. Zhai, Y. Ming, Y. Liu, and G. Zhang, "Vox-fusion: Dense tracking and mapping with voxel-based neural implicit representation," in *2022 IEEE International Symposium on Mixed and Augmented Reality (ISMAR)*. IEEE, 2022, pp. 499–507.
- [140] Z. Zhu, S. Peng, V. Larsson, W. Xu, H. Bao, Z. Cui, M. R. Oswald, and M. Pollefeys, "Nice-slam: Neural implicit scalable encoding for slam," in *Proceedings of the IEEE/CVF Conference on Computer Vision and Pattern Recognition*, 2022, pp. 12786–12796.
- [141] M. M. Johari, C. Carta, and F. Fleuret, "Eslam: Efficient dense slam system based on hybrid representation of signed distance fields," in *Proceedings of the IEEE/CVF Conference on Computer Vision and Pattern Recognition*, 2023, pp. 17408–17419.
- [142] E. Sandström, Y. Li, L. Van Gool, and M. R. Oswald, "Point-slam: Dense neural point cloud-based slam," in *Proceedings of the IEEE/CVF International Conference on Computer Vision*, 2023, pp. 18433–18444.
- [143] H. Wang, J. Wang, and L. Agapito, "Co-slam: Joint coordinate and sparse parametric encodings for neural real-time slam," in *Proceedings of the IEEE/CVF Conference on Computer Vision and Pattern Recognition*, 2023, pp. 13293–13302.
- [144] X. Huang, X. Cheng, Q. Geng, B. Cao, D. Zhou, P. Wang, Y. Lin, and R. Yang, "The apollo-scope dataset for autonomous driving," in *Proceedings of the IEEE conference on computer vision and pattern recognition workshops*, 2018, pp. 954–960.
- [145] J. Wang, J. Liu, and N. Kato, "Networking and communications in autonomous driving: A survey," *IEEE Communications Surveys & Tutorials*, vol. 21, no. 2, pp. 1243–1274, 2018.
- [146] P. Sun, H. Kretschmar, X. Dotiwalla, A. Chouard, V. Patnaik, P. Tsui, J. Guo, Y. Zhou, Y. Chai, B. Caine *et al.*, "Scalability in perception for autonomous driving: Waymo open dataset," in *Proceedings of the IEEE/CVF conference on computer vision and pattern recognition*, 2020, pp. 2446–2454.
- [147] H. Caesar, V. Bankiti, A. H. Lang, S. Vora, V. E. Liong, Q. Xu, A. Krishnan, Y. Pan, G. Baldan, and O. Beijbom, "nusenes: A multimodal dataset for autonomous driving," in *Proceedings of the IEEE/CVF conference on computer vision and pattern recognition*, 2020, pp. 11621–11631.
- [148] J. Guo, U. Kurup, and M. Shah, "Is it safe to drive? an overview of factors, metrics, and datasets for driveability assessment in autonomous driving," *IEEE Transactions on Intelligent Transportation Systems*, vol. 21, no. 8, pp. 3135–3151, 2019.
- [149] K. Muhammad, A. Ullah, J. Lloret, J. Del Ser, and V. H. C. de Albuquerque, "Deep learning for safe autonomous driving: Current challenges and future directions," *IEEE Transactions on Intelligent Transportation Systems*, vol. 22, no. 7, pp. 4316–4336, 2020.
- [150] S. Teng, X. Hu, P. Deng, B. Li, Y. Li, Y. Ai, D. Yang, L. Li, Z. Xuanyuan, F. Zhu *et al.*, "Motion planning for autonomous driving: The state of the art and future perspectives," *IEEE Transactions on Intelligent Vehicles*, 2023.
- [151] Y. Hu, J. Yang, L. Chen, K. Li, C. Sima, X. Zhu, S. Chai, S. Du, T. Lin, W. Wang *et al.*, "Planning-oriented autonomous driving," in *Proceedings of the IEEE/CVF Conference on Computer Vision and Pattern Recognition*, 2023, pp. 17853–17862.
- [152] I. Nastjuk, B. Herrenkind, M. Marrone, A. B. Brendel, and L. M. Kolbe, "What drives the acceptance of autonomous driving? an investigation of acceptance factors from an end-user's perspective," *Technological Forecasting and Social Change*, vol. 161, p. 120319, 2020.
- [153] X. Ma, W. Ouyang, A. Simonelli, and E. Ricci, "3d object detection from images for autonomous driving: a survey," *IEEE Transactions on Pattern Analysis and Machine Intelligence*, 2023.
- [154] J. Mao, S. Shi, X. Wang, and H. Li, "3d object detection for autonomous driving: A comprehensive survey," *International Journal of Computer Vision*, pp. 1–55, 2023.
- [155] D. Fu, X. Li, L. Wen, M. Dou, P. Cai, B. Shi, and Y. Qiao, "Drive like a human: Rethinking autonomous driving with large language models," in *Proceedings of the IEEE/CVF Winter Conference on Applications of Computer Vision*, 2024, pp. 910–919.
- [156] J. Wang, Y. Yuan, Z. Luo, K. Xie, D. Lin, U. Iqbal, S. Fidler, and S. Khamis, "Learning human dynamics in autonomous driving scenarios," in *Proceedings of the IEEE/CVF International Conference on Computer Vision*, 2023, pp. 20796–20806.
- [157] X. Zhou, Z. Lin, X. Shan, Y. Wang, D. Sun, and M.-H. Yang, "Drivinggaussian: Composite gaussian splatting for surrounding dynamic autonomous driving scenes," *arXiv preprint arXiv:2312.07920*, 2023.
- [158] J. Sturm, N. Engelhard, F. Endres, W. Burgard, and D. Cremers, "A benchmark for the evaluation of rgb-d slam systems," in *2012 IEEE/RSJ international conference on intelligent robots and systems*. IEEE, 2012, pp. 573–580.

- [159] J. Fang, T. Yi, X. Wang, L. Xie, X. Zhang, W. Liu, M. Nießner, and Q. Tian, "Fast dynamic radiance fields with time-aware neural voxels," in *SIGGRAPH Asia 2022 Conference Papers*, 2022, pp. 1–9.
- [160] A. Cao and J. Johnson, "Hexplane: A fast representation for dynamic scenes," in *Proceedings of the IEEE/CVF Conference on Computer Vision and Pattern Recognition*, 2023, pp. 130–141.
- [161] F. Wang, Z. Chen, G. Wang, Y. Song, and H. Liu, "Masked space-time hash encoding for efficient dynamic scene reconstruction," in *Proc. Advances Neural Inf. Process. Syst.*, 2023.
- [162] Z. Wang, A. C. Bovik, H. R. Sheikh, and E. P. Simoncelli, "Image quality assessment: From error visibility to structural similarity," *IEEE transactions on image processing*, vol. 13, no. 4, pp. 600–612, 2004.
- [163] R. Zhang, P. Isola, A. A. Efros, E. Shechtman, and O. Wang, "The unreasonable effectiveness of deep features as a perceptual metric," in *Proceedings of the IEEE conference on computer vision and pattern recognition*, 2018, pp. 586–595.
- [164] J. T. Barron, B. Mildenhall, M. Tancik, P. Hedman, R. Martin-Brualla, and P. P. Srinivasan, "Mip-nerf: A multiscale representation for anti-aliasing neural radiance fields," in *Proceedings of the IEEE/CVF International Conference on Computer Vision*, 2021, pp. 5855–5864.
- [165] K. Rematas, A. Liu, P. P. Srinivasan, J. T. Barron, A. Tagliasacchi, T. Funkhouser, and V. Ferrari, "Urban radiance fields," in *Proceedings of the IEEE/CVF Conference on Computer Vision and Pattern Recognition*, 2022, pp. 12932–12942.
- [166] Z. Xie, J. Zhang, W. Li, F. Zhang, and L. Zhang, "S-nerf: Neural radiance fields for street views," in *Proc. Int. Conf. Learn. Representations*, 2023.
- [167] H. Turki, J. Y. Zhang, F. Ferroni, and D. Ramanan, "Suds: Scalable urban dynamic scenes," in *Proceedings of the IEEE/CVF Conference on Computer Vision and Pattern Recognition*, 2023, pp. 12375–12385.
- [168] S. Peng, Y. Zhang, Y. Xu, Q. Wang, Q. Shuai, H. Bao, and X. Zhou, "Neural body: Implicit neural representations with structured latent codes for novel view synthesis of dynamic humans," in *Proceedings of the IEEE/CVF Conference on Computer Vision and Pattern Recognition*, 2021, pp. 9054–9063.
- [169] S. Peng, J. Dong, Q. Wang, S. Zhang, Q. Shuai, X. Zhou, and H. Bao, "Animatable neural radiance fields for modeling dynamic human bodies," in *Proceedings of the IEEE/CVF International Conference on Computer Vision*, 2021, pp. 14314–14323.
- [170] A. Yu, V. Ye, M. Tancik, and A. Kanazawa, "pixelnerf: Neural radiance fields from one or few images," in *Proceedings of the IEEE/CVF Conference on Computer Vision and Pattern Recognition*, 2021, pp. 4578–4587.
- [171] Y. Kwon, D. Kim, D. Ceylan, and H. Fuchs, "Neural human performer: Learning generalizable radiance fields for human performance rendering," in *Proc. Advances Neural Inf. Process. Syst.*, vol. 34, 2021, pp. 24741–24752.
- [172] C.-Y. Weng, B. Curless, P. P. Srinivasan, J. T. Barron, and I. Kemelmacher-Shlizerman, "Humannerf: Free-viewpoint rendering of moving people from monocular video," in *Proceedings of the IEEE/CVF conference on computer vision and pattern recognition*, 2022, pp. 16210–16220.
- [173] C. Geng, S. Peng, Z. Xu, H. Bao, and X. Zhou, "Learning neural volumetric representations of dynamic humans in minutes," in *Proceedings of the IEEE/CVF Conference on Computer Vision and Pattern Recognition*, 2023, pp. 8759–8770.
- [174] H. Xiong, S. Muttukuru, R. Upadhyay, P. Chari, and A. Kadambi, "Sparsegs: Real-time 360 $\{\deg\}$ sparse view synthesis using gaussian splatting," *arXiv preprint arXiv:2312.00206*, 2023.
- [175] Z. Zhu, Z. Fan, Y. Jiang, and Z. Wang, "Fsgs: Real-time few-shot view synthesis using gaussian splatting," *arXiv preprint arXiv:2312.00451*, 2023.
- [176] J. Chung, J. Oh, and K. M. Lee, "Depth-regularized optimization for 3d gaussian splatting in few-shot images," *arXiv preprint arXiv:2311.13398*, 2023.
- [177] D. Charatan, S. Li, A. Tagliasacchi, and V. Sitzmann, "pixelsplat: 3d gaussian splats from image pairs for scalable generalizable 3d reconstruction," *arXiv preprint arXiv:2312.12337*, 2023.
- [178] S. Szymanowicz, C. Ruppel, and A. Vedaldi, "Splatter image: Ultra-fast single-view 3d reconstruction," *arXiv preprint arXiv:2312.13150*, 2023.
- [179] Z. Fan, K. Wang, K. Wen, Z. Zhu, D. Xu, and Z. Wang, "Light-gaussian: Unbounded 3d gaussian compression with 15x reduction and 200+ fps," *arXiv preprint arXiv:2311.17245*, 2023.
- [180] K. Navaneet, K. P. Meibodi, S. A. Koohpayegani, and H. Pirsiavash, "Compact3d: Compressing gaussian splat radiance field models with vector quantization," *arXiv preprint arXiv:2311.18159*, 2023.
- [181] J. C. Lee, D. Rho, X. Sun, J. H. Ko, and E. Park, "Compact 3d gaussian representation for radiance field," *arXiv preprint arXiv:2311.13681*, 2023.
- [182] W. Morgenstern, F. Barthel, A. Hilsmann, and P. Eisert, "Compact 3d scene representation via self-organizing gaussian grids," *arXiv preprint arXiv:2312.13299*, 2023.
- [183] J. Gao, C. Gu, Y. Lin, H. Zhu, X. Cao, L. Zhang, and Y. Yao, "Relightable 3d gaussian: Real-time point cloud relighting with brdf decomposition and ray tracing," *arXiv preprint arXiv:2311.16043*, 2023.
- [184] Y. Jiang, J. Tu, Y. Liu, X. Gao, X. Long, W. Wang, and Y. Ma, "Gaussianshader: 3d gaussian splatting with shading functions for reflective surfaces," *arXiv preprint arXiv:2311.17977*, 2023.
- [185] Z. Yu, A. Chen, B. Huang, T. Sattler, and A. Geiger, "Mip-splatting: Alias-free 3d gaussian splatting," *arXiv preprint arXiv:2311.16493*, 2023.
- [186] Z. Yan, W. F. Low, Y. Chen, and G. H. Lee, "Multi-scale 3d gaussian splatting for anti-aliased rendering," *arXiv preprint arXiv:2311.17089*, 2023.
- [187] T. Lu, M. Yu, L. Xu, Y. Xiangli, L. Wang, D. Lin, and B. Dai, "Scaffold-gs: Structured 3d gaussians for view-adaptive rendering," *arXiv preprint arXiv:2312.00109*, 2023.
- [188] B. Lee, H. Lee, X. Sun, U. Ali, and E. Park, "Deblurring 3d gaussian splatting," *arXiv preprint arXiv:2401.00834*, 2024.
- [189] D. Malarz, W. Smolak, J. Tabor, S. Tadeja, and P. Spurek, "Gaussian splitting algorithm with color and opacity depended on viewing direction," *arXiv preprint arXiv:2312.13729*, 2023.
- [190] Z. Liang, Q. Zhang, Y. Feng, Y. Shan, and K. Jia, "Gs-ir: 3d gaussian splatting for inverse rendering," *arXiv preprint arXiv:2311.16473*, 2023.
- [191] Y. Shi, Y. Wu, C. Wu, X. Liu, C. Zhao, H. Feng, J. Liu, L. Zhang, J. Zhang, B. Zhou *et al.*, "Gir: 3d gaussian inverse rendering for relightable scene factorization," *arXiv preprint arXiv:2312.05133*, 2023.
- [192] S. Girish, K. Gupta, and A. Shrivastava, "Eagles: Efficient accelerated 3d gaussians with lightweight encodings," *arXiv preprint arXiv:2312.04564*, 2023.
- [193] Y. Fu, S. Liu, A. Kulkarni, J. Kautz, A. A. Efros, and X. Wang, "Colmap-free 3d gaussian splatting," *arXiv preprint arXiv:2312.07504*, 2023.
- [194] A. Guédon and V. Lepetit, "Sugar: Surface-aligned gaussian splatting for efficient 3d mesh reconstruction and high-quality mesh rendering," *arXiv preprint arXiv:2311.12775*, 2023.
- [195] B. P. Duisterhof, Z. Mandi, Y. Yao, J.-W. Liu, M. Z. Shou, S. Song, and J. Ichnowski, "Md-splatting: Learning metric deformation from 4d gaussians in highly deformable scenes," *arXiv preprint arXiv:2312.00583*, 2023.
- [196] H. Chen, C. Li, and G. H. Lee, "Neusg: Neural implicit surface reconstruction with 3d gaussian splatting guidance," *arXiv preprint arXiv:2312.00846*, 2023.
- [197] J.-C. Shi, M. Wang, H.-B. Duan, and S.-H. Guan, "Language embedded 3d gaussians for open-vocabulary scene understanding," *arXiv preprint arXiv:2311.18482*, 2023.
- [198] M. Qin, W. Li, J. Zhou, H. Wang, and H. Pfister, "Langsplat: 3d language gaussian splatting," *arXiv preprint arXiv:2312.16084*, 2023.
- [199] X. Zuo, P. Samangouei, Y. Zhou, Y. Di, and M. Li, "Fmgs: Foundation model embedded 3d gaussian splatting for holistic 3d scene understanding," *arXiv preprint arXiv:2401.01970*, 2024.
- [200] T. Xie, Z. Zong, Y. Qiu, X. Li, Y. Feng, Y. Yang, and C. Jiang, "Physgussian: Physics-integrated 3d gaussians for generative dynamics," *arXiv preprint arXiv:2311.12198*, 2023.
- [201] L. Meyer, F. Erich, Y. Yoshiyasu, M. Stamminger, N. Ando, and Y. Domae, "Pegasus: Physically enhanced gaussian splatting simulation system for 6dof object pose dataset generation," *arXiv preprint arXiv:2401.02281*, 2024.
- [202] Y. Sun, X. Wang, Y. Zhang, J. Zhang, C. Jiang, Y. Guo, and F. Wang, "icomma: Inverting 3d gaussians splatting for camera pose estimation via comparing and matching," *arXiv preprint arXiv:2312.09031*, 2023.
- [203] C. Pokhariya, I. N. Shah, A. Xing, Z. Li, K. Chen, A. Sharma, and S. Sridhar, "Manus: Markerless hand-object grasp capture using articulated 3d gaussians," *arXiv preprint arXiv:2312.02137*, 2023.

- [204] W. Jiang, B. Lei, and K. Daniilidis, "Fisherrf: Active view selection and uncertainty quantification for radiance fields using fisher information," *arXiv preprint arXiv:2311.17874*, 2023.